Male obesity causes adipose mitochondrial dysfunction in F_1 progeny via a let-7-DICER axis.

Chien Huang[1,2#], Joo Hyun Park[1#], Ali Altıntaş[3], Natasa Stanic[1], Kristine Kyle de Leon[1], Signe Isacson[4], Panagiotis Kalogeropoulos[5], Hande Topel Batarlar[1], Rocio Valdebenito Malmros[1], Jesper Havelund[1], Bjørk Ditlev Marcher Larsen[1], Yen-Ting Chien[2], Wen-Chi Huang[2], Karolina Szczepanowska[6,7], Jan-Wilm Lackmann[6], Aleksandra Trifunovic[6], Eva Kildall Hejbøl[8], Sönke Detlefsen[8,9], Ida Engberg Jepsen[10], Stefanie Hansborg Kolstrup[11], Ricardo Laguna-Barraza[12], Javier Martin-Gonzalez[12], Konstantin Khodosevich[13], Nils J. Færgeman[1], Marcelo A. Mori[14-17], Marc R. Friedländer[5], Anita Oest[4], Romain Barrès[3,18] and Jan-Wilhelm Kornfeld[1,19*]

[1]Department of Biochemistry and Molecular Biology (BMB), University of Southern Denmark (SDU), Odense, Denmark. [2]Laboratory of Animal Physiology, Department of Animal Science and Technology, National Taiwan University, Taipei, Taiwan. [3]Novo Nordisk Foundation Center for Basic Metabolic Research (CBMR), Faculty of Health and Medical Sciences, University of Copenhagen, Copenhagen, Denmark. [4]Division of Cell and Neurobiology, Department of Biomedical and Clinical Sciences, Linköping University, Sweden. [5]Science for Life Laboratory, Department of Molecular Biosciences, The Wenner-Gren-Institute, Stockholm University, Sweden. [6]Cologne Excellence Cluster on Cellular Stress Responses in Aging-Associated Diseases (CECAD) & Center for Molecular Medicine (CMMC), University of Cologne, Cologne, Germany. [7]IMol Polish Academy of Sciences, 02-247 Warsaw, Poland. [8]Department of Pathology, Odense University Hospital, Odense, Denmark. [9]Department of Clinical Research, Faculty of Health Science, University of Southern Denmark, Odense, Denmark. [10] The Fertility Clinic, Department of Obstetrics and Gynaecology, Zealand University Hospital, Koege, Denmark. [11]Biomedical Laboratory, Institute of Molecular Medicine, University of Southern Denmark, Odense, Denmark. [12]Core Facility for Transgenic Mice, Department of Experimental Medicine, Faculty of Health and Medical Sciences, University of Copenhagen, Copenhagen, Denmark. [13]Biotech Research & Innovation Centre (BRIC), University of Copenhagen, Copenhagen, Denmark. [14]Department of Biochemistry and Tissue Biology, Institute of Biology, Universidade Estadual de Campinas, Campinas, São Paulo, Brazil. [15]Program in Genetics and Molecular Biology, Institute of Biology, Universidade

Estadual de Campinas, Campinas, São Paulo, Brazil. [16]*Obesity and Comorbidities Research Center (OCRC), Universidade Estadual de Campinas, Campinas, São Paulo, Brazil.* [17]*Experimental Medicine Research Cluster (EMRC), Universidade Estadual de Campinas, Campinas, São Paulo, Brazil.* [18]*Institut de Pharmacologie Moléculaire et Cellulaire, Université Côte d'Azur & Centre National pour la Recherche Scientifique (CNRS), Valbonne, 06560, France.* [19]*Novo Nordisk Foundation Center for Adipocyte Signalling, University of Southern Denmark, Odense, Denmark.*

#These authors contributed equally to this work,

*Corresponding author

Abstract

We here describe that obesity and weight loss in male mice cause reversible abnormalities in glucose and lipid metabolism, serum metabolomes and lipidomes as well as expression of microRNAs, mRNAs and proteins controlling mitochondrial function in epididymal white adipose tissue. When mating obese male mice with lean females, we observed reductions in expression and translation of genes encoding mitochondrial respiratory components in (F_1) offspring that closely resemble those observed in the paternal (F_0) generation. When mapping miRNA regulation across somatic organs (i.e., liver, adipose) and sperm and $F_{0/1}$ generations, we found that obesity and weight loss reversibly affected miRNA levels, and that *let-7* isoforms were induced in obese F_0 and F_1 adipose tissue and sperm of obese F_0 mice, eliciting qualitatively similar responses in two adjacent tissues. Overexpressing *let-7* in adipocytes silenced DICER1, a miRNA processing enzyme crucial for adipose adaptation to obesity as evidenced by deficiencies in mitochondrial function following DICER1 loss in primary adipocytes. Also, microinjection of synthetic *let-7* mimetics at physiological levels found in obese sperm into zygotes from lean mice elicited glucose intolerance and impediments in adipose mitochondrial gene expression in mice sired from *let-7* microinjected zygotes, phenocopying hereditary aspects of paternal obesity. When performing single-cell RNA-Seq of miRNA-injected embryos, *let-7* impaired mitochondrial gene expression, suggesting altered oxidative metabolism following zygotic *let-7* delivery. When studying miRNA alterations in human semen, lifestyle-induced weight loss downregulated *hsa-let-7*, suggesting similar roles for human *let-7* in gametic epigenomes and embryogenesis.

57 **Introduction:**

58

59 ***Intergenerational epigenetic inheritance of metabolic dysfunction***

60 Genome-wide association studies have demonstrated that genetic (i.e., DNA) variants only explain 20%
61 of obesity heritability[1]. Given pandemic rises in obesity in evolutionarily relatively short timescales, it
62 was proposed that non-genetic or ‚*epi-genetic*‘ processes, that are spurred by obesogenic lifestyles and
63 other changes in environment exposures, might increase obesity susceptibility and contribute to disease
64 incidences. This form of epigenetic inheritance, if convincingly demonstrated[2], is particularly intriguing
65 for cases of paternal programming where affected fathers contribute only sperm as biological material
66 to embryos (intergenerational inheritance) or no genetic/biological material at all (transgenerational
67 inheritance). Epidemiological support for the existence of hereditary, paternally-acquired traits comes
68 from historical records demonstrating that ample ancestral food supplies affects cardiometabolic traits
69 up to two generations[3,4], showing that individuals carry increased risks of cardiometabolic dysfunction
70 if their parents or grandparents were obese or were malnourished[5]. In line with correlative observations
71 in human, mechanistic studies in isogenic (genetically identical) mouse strains like C57BL76
72 demonstrated that paternal obesity can impair metabolism in offsprings (F_1 generation and beyond) and,
73 specific diet like low-protein[6] or high-fat diet feeding[7-9] and stress-related cues such as depression-like
74 behavior[10], fear-conditioning[11] and psychological traumata[12] impart specific epigenetic behavioral and
75 metabolic effects in offsprings. Recently, beneficial types of epigenetic programming in adipose tissue
76 were also demonstrated where offsprings of mice exposed to cold temperatures display increased
77 amounts of metabolically favourable brown adipose tissue [13], suggesting an unexpectedly high plasticity
78 of the molecular and cellular mechanisms underlying intergenerational epigenetic responses.

79

80 ***The molecular basis for epigenetic inheritance of paternal obesity in male gametes***

81 The molecular and cellular basis for epigenetic heredity remains largely enigmatic: Although changes
82 in epigenetic marks like methylation of genomic DNA, histone post-translational modifications and
83 alterations in small Noncoding RNAs (sncRNAs) correlate with hereditary processes in male gametes[14].
84 Although lifestyle/diet-induced changes to DNA methylation and histones modifications were reported,

85 the evidence for causatively implicating these in eliciting paternal response in progeny is rare for higher
86 mammalian species like rodents and humans. Other emerging instigators of intergenerational response
87 are found amongst the different types of gametic sncRNAs such as microRNAs (miRNAs): miRNAs in
88 gametes were initially identified and functionally dissected in nematodes and fruit flies[15-18], thus species
89 where sncRNAs-evoked gametic gene silencing processes are well-understood [19]. In contrast to DNA-
90 linked marks, sncRNAs are very mobile in nature and are subject to microvesicular trafficking between
91 cells and organs and secreted by somatic cell types in testes[20,21]. Thus, due to their high abundance of
92 miRNAs in sperm, their dynamic changes following diet exposures[22,23], their exchange between sperm
93 and oocytes[23] sperm-born sncRNAs have the unique potential for exchanging information about past
94 lifestyle choices to zygotes and F_1 progeny. Consistent with this, metabolic trait/disease-associated
95 miRNAs can affect intergenerational phenotypes and phenocopy F_0 lifestyles if microinjected [24,25] or
96 removed from zygotes[26]. Beyond controlling gametic epigenomes, miRNAs are also essential for germ
97 cell development processes such as spermatogenesis[27] and embryogenesis[28], and miRNA are exchanged
98 between zygotes and other cell types [12,25,29-31]. Taken together, it is plausible to hypothesize that obesity-
99 evoked changes in sperm miRNAs alter zygotic miRNA pools and embryonic development, instigating
100 epigenetic phenotypic traits and somatic gene expression in offsprings. As diverse paternal lifestyle
101 exposures ranging from inflammation[15], nutrition[29,31] to stress [12,30] alter gametic miRNA repertoires and
102 F_1 phenotypes in non-overlapping ways, the intriguing possibility exists that environmental experiences
103 are encoded in individual gametic sncRNA signature and that these sperm sncRNAs have the potential
104 to transmit complex lifestyle exposures given the high bandwidth of RNA-mediated effects[32].
105
106 ***Regulation of adipose tissue (mitochondrial) function by miRNAs***
107 Adipose tissue is a multifunctional endocrine organ that coordinates tissue-level (autocrine, juxtacrine,
108 paracrine) and systemic (endocrine) responses by release of adipokines, lipids and inflammatory factors
109 and, shown recently, miRNA-containing microvesicles (exosomes)[33-35]. It is believed that adipose tissue
110 can safely store ingested nutrients as lipids, although chronic calorie excess causes insulin resistance[36],
111 aberrant gene expression in adipocytes[37], vascular remodelling and immune cell infiltration[33].
112 Mitochondria in adipose tissue exert important functions for tissue/energy homeostasis, particularly

113 during nutrient deprivation/excess[35]: Whereas brown adipose tissue (BAT) contains large numbers of
114 mitochondria to generate heat by dissipation of the electron transport chain (ETC) proton gradients[38],
115 inguinal (beige, iWAT) and epididymal (white, eWAT) adipose tissue protects from calorie overload
116 by removing nutrients from circulation and storage as energetic, indolent macromolecules such as
117 triglycerides. Mitochondrial function in WAT is impaired in obesity [39] and reduced mitochondrial
118 function in fat causes metabolic imbalance[40-43]. Mitochondrial DNA content, oxidative phosphorylation
119 (OxPhos), abundance and composition of ETC complexes are all functionally impaired in obesity and
120 morphological aberrations in mitochondrial structures are found in obesity[39,43] and aging[44]. Conversely,
121 treatment with the AMP-activated protein kinase (AMPK) agonist Metformin improves mitochondrial
122 function in adipose tissue, as do exercise or calorie restriction, and all these interventions correlate with
123 metabolic improvement[45]. Recently, miRNAs were identified as important regulators of mitochondrial
124 formation and function and known ‚mito-miRs' like *miR-143, miR-181a, miR-378* instigate, whereas
125 *miR-532* which impairs mitochondrial function by (post-transcriptionally) silencing mitochondrial
126 translocation and mt-RNA homeostasis[46-48]. We and others showed that removing miRNAs from
127 adipocytes by conditionally ablating DICER1, a central component of the conserved miRNA processing
128 machinery, impairs adipogenesis, triggering lipodystrophy and metabolic dysfunction in mice[49-51].
129
130 Collectively, we report that obesity in male mice is linked to reversible miRNA, mRNA and proteins
131 alterations in adipose mitochondrial gene regulation that match those in adipose tissue of lean isogenic
132 F_1 progeny. Using integrative analyses of adipose, liver and sperm miRNA:mRNA gene networks, we
133 identify *let-7* as induced by obesity across cell types and generations and mechanistically implicate *let-*
134 *7* driven suppression of DICER1 and concomitant declines in mitochondrial function in adipocytes in
135 inherited mouse phenotypes, thereby establishing sperm-born *let-7* as intergenerational driver of
136 mitochondrial dysfunction and glucose impairments in F_1 offspring.

137 **Results**

138 ***Paternal obesity elicits intergenerational impairments in adipose mitochondrial function***

139 Whilst intergenerational effects of paternal (F_0) obesity on offspring (F_1) phenotypes and metabolic
140 health have been reported, the specific organ-level manifestations of this dysfunction in progeny, and
141 the precise somatic and germ cell-intrinsic molecular mechanisms in obese mice and their descendants,
142 remain surprisingly elusive. To investigate this using isogenic rodents (*Mus musculus*), we used diet-
143 induced obese (DIO) and weight-regressed C57BL/6N male mice, and fed 6-week-old animals with 1)
144 low-fat diet (LF) for 18 weeks (F_0 LF), 2) high-fat diet (HF) for 18 weeks (F_0 HF) or 3) HF for 9 weeks,
145 followed by 9 weeks of LF-driven weight loss (F_0 HF-LF, **Fig.1a**) to allow at least three cycles of
146 spermatogenesis. For each F_0 group, we mated eight randomly selected mice with unexposed lean
147 virgin, female C57BL/6N mice, and exposed both male and female F_1 progeny of each group, i.e., F_1
148 (F_0 LF, n=44 pups), F_1 (F_0 HF, n=52 pups) and F_1 (F_0 HF-LF, n=38 pups) mice to LF after weaning to
149 test for metabolic and metabolic sequelæ of F_0 diet exposure and removal. We did not additionally
150 challenge F_1 mice with HF given that effects of HF and epigenetic F_0 effects were reported as
151 cumulative with regards to F_1 phenotypes [52] (**Fig.1b**). Noteworthy, we detected no alterations in
152 fecundity, male-to-female pup ratio and litters sizes (**Fig.S1a,b**), suggesting that F_0 obesity did not
153 affect development and embryonic implantation rates nor indirectly affected maternal provisioning after
154 birth due to different litter sizes, two potential confounders.

155

156 When phenotyping F_0 and male F_1 animals for metabolic traits commonly associated with obesity and
157 type 2 diabetes (T2D), we found that HF increased and ensuing HF-LF feeding reduced body weight to
158 levels seen in F0 LF mice, whilst F_1 progeny were indistinguishable in terms of body weight (**Fig.1c**).
159 Intriguingly, male obesity impaired glucose tolerance (**Fig.1d, Fig.S2a**) and insulin sensitivity (**Fig.1e)**
160 not only in F_0 HF mice, but also in their F_1 (F_0 HF) offsprings without changes in circulating F_1 insulin
161 (**Fig.S2b**) and no alterations in liver and brown adipose tissue mass (not shown). In contrast, we found
162 that obesity increased iWAT (**Fig.S2c**) and eWAT (**Fig.1f**) masses and elevated serum levels of leptin,
163 an important adipokine reflecting adipocyte size and numbers, in F_0 and F_1 mice (**Fig.1g**). Adipocyte
164 size determination using haematoxylin/eosine (H/E) staining of formalin-fixated, paraffine-embedded

165 adipose sections demonstrated comparable shifts towards increased eWAT adipocyte sizes in F_0 and F_1
166 (**Fig.1h-j**), suggesting that paternal obesity might promote lipid accrual/lipolysis as well as metabolic
167 processes governing adipocyte health by similar molecular mechanisms in both generations and via this
168 mechanism contribute to glucose intolerance in F_0 and male F_1. When phenotyping female offsprings
169 of lean, obese and weight-regressed F_0 fathers, we observed no changes in F_1 weight (**Fig. S2d**), mild
170 glucose intolerance (**Fig.S2e,f**) and only trends towards changes in insulin sensitivity (**Fig.S2g**). In
171 support of overall mild impairments in female offsprings, random fed glycemia (**Fig.S2h**) and organ
172 weights (**Fig.S2i**) were also unchanged in female progeny. *Thus, male obesity and weight loss reversibly*
173 *affect glucose tolerance in F_1, with metabolic effects predominantly observed in male progeny.*
174
175 For comprehensive insights into molecular processes affected by paternal obesity and weight loss, and
176 those governing intergenerational effects, we performed bulk tissue mass spectrometry to determine
177 differentially abundant proteins in F_0 and F_1 eWAT. We observed 980/431 proteins increased in F_0 HF
178 compared to F_0 LF mice and in F_1 (F_0 HF) compared to F_1 (F_0 LF) mice. Conversely, 632/305 proteins
179 were less abundant comparing F_0 HF to F_0 LF mice (**Fig.S3a**) and F_1 (F_0 HF) compared to F_1 (F_0 LF)
180 mice (**Fig.S3b**). Using the STRING database (https://string-db.org/) followed by Gene Ontology (GO)
181 analysis of overrepresented biological processes (GOBP), we intriguingly saw that F_0 HF mice (**Fig.1k**)
182 and F_1 (F_0 HF) progeny (**Fig.1l**) shared the same downregulated, mitochondria-associated GOBPs such
183 as Oxphos, adenosine triphosphate (ATP) synthesis, and regulation of ETC subunits. Examples of
184 proteins similarly repressed in F_0 HF and F_1 (F_0 HF) eWAT included components of ETC Complex I
185 like NADH dehydrogenase 1 alpha subcomplex subunit 8 (NDUFA8) and NADH dehydrogenase iron-
186 sulfur protein 6 (NDUFS6), of Complex IV like Cytochrome C Oxidase Subunit 6B1 (COX6B1), of
187 mitochondrial membrane-intrinsic lipid carriers such as *Carnitine Palmitoyltransferase 1A* (CPT1A)
188 and of mitochondrial protein translocation such as *Translocase Of Outer Mitochondrial Membrane 20*
189 (TOMM20). In contrast, upregulated GOBP terms in F_0 HF mice (**Fig.S3a**) and their F_1 (F_0 HF) progeny
190 (**Fig.S3b**) included unrelated GOBP terms like protein translation, Golgi-mediated transport and
191 secretion as well as protein localisation. Importantly, abundance of metabolite- (**Fig.S4a-c**) and lipid-
192 based (**Fig.S4d,e**) biomarkers that can reflect systemic mitochondrial dysfunction, for instance tricarbon

193 cycle acid (TCA) intermediates like citrate, malate, fumarate, alpha-ketoglutarate and citrate, were
194 reduced by paternal obesity and restored by weight loss (**Fig.S4f**) and mitochondrial lipid carriers like
195 (acetylated) carnitine (**Fig.S4g**) were reduced. Furthermore, saturated, short-chain C:16:0/C:18:0
196 ceramides, i.e., lipid species reported to disrupt mitochondrial function and elicit mitochondrial ER
197 stress in obese adipocytes[53,54] were induced, whilst mito-protective long-chain C18:1/C24:1 ceramides
198 were reduced in F_0 HF mice (**Fig.S4h**). *Thus, male obesity downregulates proteins associated with*
199 *mitochondrial processes in obese F_0 and F_1 offsprings that correlate with reduced levels of*
200 *mitochondrial function and lipid catabolism, likely reflecting a system-wide hereditary form of*
201 *mitochondrial dysfunction, also in adipose tissue.*
202
203 ***Paternal obesity negatively affects expression of mitochondria-associated miRNA-mRNA networks***
204 We next turned our attention to in detail study gene-regulatory processes at the messenger and miRNA
205 level that might underly the observed repression of mitochondria-associated proteins in F_0 and F_1
206 adipose tissue, and to this end performed mRNA-seq of eWAT and liver of F_0 and F_1 groups and
207 performed miRNA and mRNA differential expression analysis, specifically focussing on mitochondrial
208 processes. Comparing F_0 HF to F_0 LF eWAT using adjusted p-Values (pV_{adj}) $\leq$0.05 we detected yielded
209 3,265 up-regulated and 2,890 down-regulated genes (**Fig.2a**). When comparing F_1 (F_0 HF) to F_1 (F_0 LF)
210 mice we detected no significantly regulated genes when accounting for multiple testing (pV_{adj}). Yet
211 when specifically interrogating differential expression to reflect the more variable transcriptional effects
212 in F_1 mice, we found 766 up-regulated and 893 down-regulated genes using unadjusted p-Values (pV)
213 $\leq$ 0.05 (**Fig.2b**). When performing gene set enrichment analysis (GSEA) of affected GOBP we found
214 upregulated processes linked to cell proliferation and immune activation that likely reflect adipocyte
215 hyperplasia and inflammation, thus cellular processes commonly associated with obesity, and GOBP
216 associated with germ cell and cilial function in F_1. Importantly, we confirmed our proteomic findings
217 and detected overrepresented GOBP related to lipid catabolism, ATP synthesis, OxPhos and ETC
218 downregulated in adipose tissue of F_0 HF mice (**Fig.2c**) and their F_1 offsprings (**Fig.2d**) and, when
219 interrogating expression of mRNAs encoding mitochondrial ETC I-V, we confirmed the repression of
220 nuclear-expressed mitochondrial constituents at the mRNA level (**Fig.2a,b**). Importantly, aberrant

221 mitochondrial effects were to large extends reversible by weight loss, as comparing F_0 HF to F_0 HF-LF
222 eWAT yielded 2,687 up-regulated and 2,237 down-regulated using pV_{adj} (**Fig.S5a**), whilst comparing
223 F_1 (F_0 HF) to F_1 (F_0 HF-LF) eWAT yielded 547 up-regulated and 732 down-regulated genes without
224 adjusting for multiple testing, (**Fig.S5b**) and GOBP restored by weight loss also fell into genes linked
225 to mitochondrial function (**Fig.S5c,d**).
226
227 Given that miRNAs are important (rheostatic) components in post-transcriptional gene network and
228 have previously been linked to mitochondrial maturation and function[55], albeit not in adipocytes, we
229 next wondered whether concerted down-regulation of mitochondrial programs in obese eWAT might
230 (partially) be instigated by altered expression of mito-miRs[1]' like *let-7*[2], *miR-378*[3], *miR-181*[4], *miR-143*[5]
231 that functionally support mitochondrial formation and oxidative metabolism. Thus, when conducting
232 small RNA (sRNA)-seq to determine differential miRNA expression, we found that F_0 obesity repressed
233 mito-miRs that positively affect mitochondrial biogenesis and function, for instance *miR-143-3p*[56], *miR-*
234 *181a-2-3p*[57,58], *miR-182*[59], *miR-200*[60] and *miR-378a-3p*[61] in eWAT of F_0 HF (**Fig.2e**) and F_1 (F_0 HF,
235 **Fig.2f**) mice, whereas mitochondria-inactivating *miR-532*[62] was induced in F_0 HF (**Fig.6c**) and F_1 (F_0
236 HF, **Fig.6d**) eWAT, suggesting that miRNA dysregulation contributed to mitochondrial impediments
237 observed in obese F_0 eWAT. Integration of miRNA-mRNA NGS datasets with adipocyte-specific
238 miRNA-mRNA-Argonaute 2 interactomes using AGO-HITS-CLIP[6] revealed that *miR-378 and miR-*
239 *143*, despite being predicted, did not coinidce with downregulation of their mitochondrial protein targets
240 (**Fig.2g**), whilst *miR-532-5p* was both predicted to target and observed to coincide with mitochondrial
241 proteins repressed in F0 obesity, arguing for roles of *miR-532,* but not *miR-143/378* in driving
242 mitochondria dysfunction in F_0 HF eWAT (**Fig.2h**). In line with body weight loss-driven mRNA
243 transcriptional responses (**Fig.S6a,b**), miRNA alterations were highly dynamic, and weight loss
244 restored expression of mitochondria-promoting in F_0 HF (**Fig.S5e**) and F_1 (F_0 HF, **Fig.S5f**) mice. *Thus,*
245 *F_0 obesity causes reversible repression of mitochondrial and lipid catabolic genes, and miRNA-mRNA*
246 *network analysis implicates obesity-regulated mito-miRs in this process.*
247
248 ***The specificity of obesity-induced heritable epigenetic mitochondrial alterations to adipose tissue***

249 We were in the following interested to address how confined the observed heritability of mitochondrial
250 dysfunction was i. as a cellular and metabolic process and to ii. adipose tissue and performed mRNA-
251 seq to assess the heredity of other obesity-associated processes such as chronic, low-grade inflammation
252 (meta-inflammation). Focussing on expression of gene markers of classically (M1) and alternatively
253 activated (M2) monocytes/macrophages, cell types that are linked to meta-inflammation-driven adipose
254 tissue dysfunction[33], we found that, as expected, mRNAs encoding M1 markers such as *Interleukin 1b*
255 *(IL1b)*, *Monocyte chemoattractant protein-1 (Mcp1/Ccl2)* and *Tumor Necrosis Factor Alpha (TNF)*;
256 but also M2 markers like *Arginase 1 (Arg1)*, *Mannose Receptor C-Type 1 (Mrc1)*, *C-Type Lectin*
257 *Domain Containing 10A (Clec10a)* and *Resistin Like Beta (Retnla)* were induced in F_0 HF, but not F_1
258 eWAT (**Fig.S6e,f**), emphasising that a meta-inflammatory tone is not passed on from F_0 HF mice.
259
260 Given the dysfunction in a specialised cellular process like mitochondrial respiration in eWAT, we next
261 aimed to juxtapose adipose tissue with transcriptional effects in liver, an organ essential for glucose and
262 lipid homeostasis: Analysis of mRNAseq data using multidimensional scaling (MDS) plots showed that
263 F_0 LF segregated from F_0 HF and F_0 HF-LF, arguing for mostly irreversible effects of obesity in F_0 liver
264 (**Fig.S7a**) and modest effects of F_0 obesity on F_1 liver transcriptomes (**Fig.S7b**). When comparing F_0
265 HF to F_0 LF livers, we found 2,474 up- and 2,612 down-regulated genes with $pV_{adj} \leq 0.05$ (**Fig.S7c**),
266 whereas comparing F_1 (F_0 HF) to F_1 (F_0 LF) without adjusting for multiple testing ($pV \leq 0.05$) yielded
267 716up- and 546 down-regulated genes (**Fig.S7d**). Gene Set Enrichment analysis (GSEA)[63] of
268 differentially regulated mRNAs identified lipid metabolism and organelle formation as induced,
269 whereas repressed terms included lipoprotein trafficking, endoplasmic reticulum and ribosome, yet no
270 transcriptional evidence for altered mitochondrial processes in liver of obese mice and their F_1 progeny
271 (**Fig.S7e,f**), emphasising the specificity of mitochondrial alterations in obese fat.
272
273 The non-hereditary effects of paternal obesity were supported by histological evidence, and pathologist
274 assessment of H/E (morphology), Sirius Red (collagen/fibrosis) and anti-CD45 (leukocytes) staining
275 revealed important hallmarks of metabolic dysfunction-associated steatosis liver disease (MASLD) like
276 micro-/macro-vesicular steatosis, fibrosis and locular inflammation in F_0 HF mice, but not lean F_0 or F_1

277 descendants (**Fig.S8a-h**). Targeted analysis of expression changes in genes linked to hepatic lipid
278 metabolism and meta-inflammation such as *Adhesion G Protein-Coupled Receptor E1 (Adgre, F4/80)*,
279 *Apolipoprotein A4 (Apoa4), Apolipoprotein E (Apoe), Low Density Lipoprotein Receptor (Ldlr),*
280 *Peroxisome Proliferator Activated Receptor Gamma (Pparg), Cluster of Differentiation 36 (Cd36)* and
281 *Sterol Regulatory Element Binding Transcription Factor 1 (Srebf/Srebp1)* confirmed that induction was
282 confined to F_0 HF livers (**Fig.S8i**). Furthermore, mitochondria-associated genes that were activated in
283 obesity, presumably counteracting lipid accumulation in MASLD, for instance *Carnithine*
284 *Palmitoyltransferase 1A (Cpt1a)*, *Carnithine O-Acetyltransferase (Crat), Acyl-Coa-Oxidase (Acox1)*
285 and *Acetyl-CoA-Acetyltransferase (Acat1)* were induced in livers from F_0 HF, but not F_1, mice. *Thus,*
286 *combinatorial analyses of transcriptional and histological changes argue against prominent effects of*
287 *paternal obesity onto F_1 gene expression and mitochondrial processes in hepatic cell types.*
288
289 ***Paternal obesity causes qualitatively similar alterations in eWAT and sperm of obese male mice***
290 Spermic sncRNA were reported to be subjected to dietary cues such as high-fat and -sugar diets in mice
291 and humans[22]; and it is therefore conceivable that HF feeding and weight loss alter spermic sncRNA
292 levels that can then, following oocyte fertilisation, be passed on to fertilised oocytes (zygotes) as shown
293 recently [23]. By changing sRNA composition in zygotes, sncRNAs thus have the unique ability to post-
294 transcriptionally affect decision points in embryogenesis, thereby contributing to the observed glucose
295 intolerance and mitochondrial protein repression observed in F_1 offsprings sired by F_0 HF bucks. A
296 particular aspect of sperm transcriptomes is the complex profile of sncRNAs involving miRNAs,
297 ribosomal RNAs (rRNAs), PIWI-interacting RNAs (piRNAs), (mitochondrial) transfer RNAs ((mt)-
298 tRNAs) and (mt)-tRNA fragments [26] that, as described by Tomar et al.[23], are affected by mitochondrial
299 dysfunction in obesity and, particularly relevant in this setting, are physically exchanged between sperm
300 and oocytes during fertilisation, a scenario also conceivable for other types of mitochondria-associated
301 sncRNAs, for example mito-miRs. To the map the effects of paternal obesity and weight loss on spermic
302 sncRNAs and to gain insights into sRNA-driven metabolic adaptations in F_0 HF sperm, we next isolated
303 motile spermatozoa using swim-up assays and charted differential spermic sncRNAs responses as
304 consequence of body weight gain and losses and found sperm harboured complex sncRNA pools of

305 thousands of (mt)-tRNAs, piRNAs, rRNAs and miRNAs (**Fig.3a-c**). In addition to effects elicited by
306 obesity and/or LF feeding at the single sncRNA level, we observed that (mt)-tRNAs and miRNAs as
307 entire RNA biotype were repressed by HF feeding. As a prior study from Tomar et. al[23] had shown
308 effects on mt-RNA in sperm after HF feeding, this was investigated further: Mt-tsRNA fragments were
309 found for nine mt-tRNAs (*mt-Tl1*, *mt-Tq*, *mt-Tm*, *mt-Ts1*, *mt-Tr*, *mt-Th*, *mt-Ts2*, *mt-Te*, *mt-Tp*), where
310 mean cpm above 10 was observed in *mt-Tm*, *mt-Ts1*, *mt-Ts2* and *mt-Th* (**Fig.9a**), but only 5' fragments
311 of *mt-Ts-1* were significantly changed in sperm from F_0 HF and F_0 HF-LF diet (**Fig.9b**). As miRNAs
312 are abundant in somatic cell types and sperm, harbour the possibility of horizontal transfer between
313 them, and exert gene-regulatory functions within both cellular compartments, we turned our attention
314 to miRNA regulation in sperm. We found that F_0 obesity and weight loss caused a coordinated and
315 inverse (i.e., downregulation and upregulation, respectively) effects on miRNome regulation (**Fig.3d,e**),
316 a finding previously observed by our labs [51] and others[49,50,64] for obese adipose tissues; in the latter case
317 at least partially due reduced abundance of DICER1. Intrigued by the repression of miRNAs in two
318 functionally distinct, yet anatomically adjacent tissues and cell types like eWAT and sperm, we asked
319 if differential miRNA responses were qualitative similar in both organ which, if present, would support
320 the possibility of physical miRNA exchange between eWAT adipocytes and sperm as shown for other
321 testicular cell types and sperm[21]: Indeed, upon comparison of lean, obese and weight-regressed sperm
322 and eWAT miRNAs, we found highly congruent responses across both compartments with activating
323 mito-miRNAs like *miR-378* and *miR-143* being down-regulated, whilst inactivating mito-miRs of the
324 *let-7* family up-regulated in obese F_0 eWAT and sperm (**Fig.3f)**. Importantly, when broadly mapping
325 the regulation of *let-7* family isoforms, we found mild, but synchronous inductions of *let-7* in F_0 eWAT
326 and sperm and F_1 eWAT (**Fig.3g-3i**). As increases of *let-7c* were reported in intergenerational rat studies
327 by us [8] and others[65] and because *let-7* impairs embryo implantation and glucose homeostasis when
328 overexpressed in mice [66,67], we focussed on *let-7* isoforms for functional follow-up studies in germ cells
329 and adipocytes. *Thus, paternal obesity triggers similar alterations in adipose tissue and sperm miRNAs*
330 *and let-7 isoforms are consistently induced across cell types and generations.*
331
332 ***Zygotic delivery of let-7 causes glucose intolerance and mitochondrial impairment in sired mice***

333 Prompted by profound and reversible effects of male obesity and weight loss on sperm miRNomes and
334 *let-7* in particular, as environmentally and artificially induced (e.g., elicited by miRNA microinjection)
335 alteration in zygote miRNA (pools) trigger abnormalities in progeny[25,68], and because embryonic
336 trajectories require maturation of pre- into mature miRNAs[69], we tested the functional relevance of *let-*
337 *7* gain-of-function in one-cell embryos for F_1 phenotypes. We focussed on *let-7d-5p* and *let-7e-5p* given
338 that these exhibit the most concordant increases amongst *let-7* family members in F_0 and F_1 eWAT and
339 sperm (**Fig.3g-i**) and because *let-7* has before been connected to embryonic cell fate decisions[70,71]. To
340 test if zygotic delivery of *let-7* corresponding at levels seen in few obese spermatozoa triggers
341 phenotypical and metabolic changes in mice sired from *let-7* microinjected embryos (F_{MI} generation)
342 and whether these would resemble mice sired by F_0 HF fathers, we injected physiological amounts (50
343 fmol, i.e., *let-7* found in 5-10 spermatozoa) of *cel-mir-67* mimic as non-mammalian (*C.elegans*) control,
344 and mimics for *let-7d-5p* and *let-7e-5p* by microinjection into zygotes conceived from lean males and
345 females C57BL/6N mice using standard protocols[29] (**Fig.4a**). We injected 126/138/106 zygotes with
346 *cel-mir-67*, *let-7d-5p* and *let-7e-5p*, but observed no discernible difference in implantation success, litter
347 sizes and number of pregnancies in F_{MI} mice (**Fig.S10**), arguing against roles of *let-7* for zygote viability
348 and implantation. Next, we analysed at least 19 pups per group from 3-4 pregnancies but observed no
349 overt differences in postnatal body weight trajectories (**Fig.4b**). Despite similar weight, we detected
350 impaired glucose tolerance (**Fig.4c,d**), insulin resistance (**Fig.4e**) and elevated random-fed glycemia
351 **(Fig.4f)** in mice sired by *let-7* injected F_{MI} embryos, whilst eWAT and liver weights were
352 indistinguishable between F_{MI} groups (**Fig.4g**). Importantly, when performing mRNA-seq in eWAT of
353 F_{MI} mice, despite mild changes, we found that *let-7* down-regulated mitochondrial processes in F_{MI} mice
354 (**Fig.4h**). *Thus, zygotic delivery of let-7 at levels corresponding to few F_0 HF sperm cells, causes*
355 *glucose intolerance and aberrant mitochondrial gene regulation in mice derived from these embryos.*
356

357 ***Obesity-associated let-7 rewires mitochondrial metabolism during embryogenesis***

358 As transfer of miRNA perturbation in sperm to oocytes can have deleterious consequences and give
359 rise to incompletely developed embryos [20,72,73], and as zygotes and blastocysts have the capacity to
360 differentiate into virtually all cell types, (early) embryogenesis represents an important window of

361 developmental plasticity that might affect F_{MI} phenotypes if perturbed by miRNA delivery, despite the
362 physiological levels of miRNA delivery and absence of embryonic lethality. Nonetheless, it is
363 conceivable that alterations in zygotic miRNAs still entails far-reaching consequences in sired mice due
364 to a combination of altered developmental, epigenetic and metabolic processes[73]. Based on the specific
365 mitochondrial alterations, but absence of increased *let-7* levels in F_{MI} eWAT, we next hypothesized that
366 *let-7d-5p* and *let-7e-5p* could carry out important roles in cell fate decisions during embryogenesis
367 which will indirectly contribute to the glucose intolerance in F_{MI} pups via altered embryonic
368 development. To test this experimentally, we repeated zygotic *let-7* injections but allowed miRNA-
369 injected embryos to divide thrice until the 8-cell blastomere stage. We dissociated embryos into single
370 blastomeres and performed single-cell RNA-Seq (scRNA-seq) using Smart-seq2[74] (**Fig.4i**).
371 Remarkably, we found that after three cell divisions, miRNA-injected blastomeres were still
372 transcriptionally distinct, reflecting the profound transcriptional and developmental consequences of
373 inducing *let-7* in zygotes (**Fig.4j**). When performing GSEA of *let-7*-dependent gene sets, we
374 corroborated that *let-7d-5p* repressed terms linked to mitochondrial processes like ATP synthesis, TCA
375 cycle and ETC (**Fig.4k**). Intergenerational programming in isogenic rodents has been described before,
376 yet it is elusive if these effects are translatable to species with highly different reproductive apparatuses,
377 genetic backgrounds, and timescales of obesity development like humans. Although epidemiological
378 evidence[4,75] suggests heritable effects of overfeeding and malnutrition in humans (e.g., the famous
379 'Dutch Hunger Winter'[76]), causal evidence for epigenetic inheritance is hard to separate from cultural
380 and ecological inheritance in humans[2]. As it is becoming appreciated that nutritional and metabolic cues
381 shape human sncRNA expression[22], we tested effects of weight change on semen *let-7* in a small cohort
382 of n=15 obese men (BMI, 39.49 ± 1.80) undergoing voluntary weight loss[77] and quantified *hsa-let-7*
383 using TaqMan qPCR. Intriguingly, we found that *hsa-let-7d-5p* and *hsa-let-73-5p* followed the trends
384 observed for weight regulation , suggesting similar correlations between metabolic improvement and
385 *let-7* reductions in human semen (**Fig.4l,m**). *Thus, obesity-associated let-7d affects murine*
386 *embryogenesis by impairing mitochondrial gene regulation and similar processes might be occurring*
387 *following weight loss in obese humans.*
388

389 ***Adipocyte let-7 impairs mitochondrial function via post-transcriptional silencing of DICER1***

390 Beyond F_0 HF sperm (**Fig.3g-i**), we found *let-7d-5p* and *let-7e-5p* upregulated in F_0/F_1 eWAT, and
391 AGO2-CLIP interactome analyses confirmed that *let-7* gene targets are enriched for genes encoding
392 mitochondrial proteins, that are downregulated by obesity in F_0/F_1 eWAT (**Fig.5a**). For this, and to add
393 to their previously ascribed role in fertilized oocytes, we aimed to dissect the transcriptional and
394 functional consequences of elevated *let-7* in adipocytes, with a specific focus on mitochondrial gene
395 regulation as highly sequence-related *let-7i* can impair commitment of mitochondria-rich adipocytes [78].
396 Yet, if roles for *let-7* in mitochondrial formation and function exist in mature adipocytes is unknown.
397 To test this, we delivered by reverse lipofection mimetics for *let-7d-5p* and *let-7e-5p* and *cel-mir-67*
398 into stromal vascular fraction-derived mature epididymal white adipocytes (1°eWA) to mimic obesity-
399 associated increased in *let-7* in eWAT. When interrogating the effects of *let-7* overexpression, we
400 observed that *let-7d-5p* elicited more pronounced effects (1,768 up-regulated, 1,387 down-regulated
401 genes, **Fig.5b**) than *let-7e-5p* (557 up-regulated, 893 down-regulated genes, **Fig.5c**) compared to *cel-*
402 *mir-67*, yet both *let-7* isoforms downregulated processes related to lipid metabolism, Insulin-AKT
403 (Protein Kinase B) signalling and carbohydrate metabolism (**Fig.S11**). Although not overrepresented at
404 the GOBP level, we found rate-limiting genes in glycolysis, TCA, and mitochondrial lipid import like
405 Carnithine Palmitoyltransferase 2 (*Cpt2*), Carnithine O-Acetyltransferase (*Crat*), Hexokinase 2 (*Hk2*),
406 Isocitrate Dehydrogenase 2 (*Idh2*), Pyruvate Carboxylase (*Pcx*), Pyruvate Dehydrogenase Kinase 2
407 (*Pdk2*) and mitochondrial ATP-magnesium/phosphate antiporter Solute Carrier Family 25 Member 24
408 (*Slc25a24*, **Fig.5b,c**; in blue) repressed upon *let-7* delivery. Importantly, we also detected pivotal genes
409 in miRNA maturation such as Ribonuclease III DICER1 *(Dicer1)* and Argonaute RISC Catalytic
410 Complex 2 *(Ago2,* **Fig.5b,c**; in red*)*. Next, we experimentally validated these predicted *let-7* targets by
411 dual luciferase reporter assays (DLRA)-based miRNA-mRNA 3'UTR interaction studies in HEK293
412 cells for genes linked to mitochondrial lipid and ATP uptake (*Slc25a24, Cpt2*), glycolysis (*Hk2*, *Pdk2*),
413 TCA activity (*Sdha*, **Fig.5d**) and miRNA processing (*Dicer1, Ago2*).

414

415 *Dicer1* 3'UTRs and exons harboured several independent *let-7* seeds of which, after mutation of
416 putative *let-7* responsive elements (MREs), two from exonic regions became refractory to *let-7*

417 repression, demonstrating direct negative effects of *let-7* on DICER1 translation (**Fig.5e**). We strived
418 to validate *let-7* targets identified in HEK293 cells adipocytes, and delivered *let-7* and control mimics
419 to 1°eWA and confirmed that *let-7* also repressed DICER1 in white adipocytes, yet caused only modest
420 reductions in mitochondria-/TCA-/glycolysis-associated proteins upon overexpression (**Fig.5f-h**),
421 prompting us to hypothesize that the chronic *let-7* induction seen in obese adipocytes might repress
422 mitochondrial function rather via sustained DICER1 loss than by direct *let-7* effects on mitochondrial
423 function; and that *Dicer1* inactivation might be a better proxy for mimicking the prolonged upregulation
424 in *let-7d-5p* and *let-7e-5p* in obesity than acute overexpression of the miRNA.
425
426 To address if *Dicer1* silencing because of sustained *let-7* upregulation is sufficient to phenocopy *in vitro*
427 the obesity-evoked impediments in mitochondrial function, we designed two independent *Dicer1*-
428 targeting locked nucleic acid (LNA) inhibitors that repressed *Dicer1* at the mRNA and protein level,
429 yet with varying efficiencies (**Fig.5i**) and interrogated mitochondrial respiration using Seahorse. We
430 found that *Dicer1* knockdown reduced oxygen consumption rates (OCR) as proxy for mitochondrial
431 respiration (**Fig.5j**) and extracellular acidification rates (ECAR) as proxy for glycolytic rates in 1°eWA
432 (**Fig.5k**) supporting our hypothesis that obesity impairs mitochondrial respiration and gene regulation,
433 at least partially, by post-transcriptional silencing of DICER1 via *let-7* (**Fig.5l**). *Thus, obesity-*
434 *associated let-7 impairs mitochondrial oxidative respiration by silencing of DICER1 in mature*
435 *adipocytes.*
436

437 **Discussion:**

438 ***High transcriptional plasticity of mitochondrial dysfunction in adipose tissue***

439 In our study we found that hepatic expression changes inflicted by HFD feeding where to a large extend
440 irreversible, whereas adipose tissue miRNA/mRNA transcriptomes and translatomes, and particularly
441 mitochondrial OxPhos and TCA gene sets, reverted to a state *ante*. Similar studies have investigated
442 the effects of reversible (i.e., diet- and exercise-evoked weight gain and loss) on hepatic and adipose
443 transcriptomes: Gonzalez-Francesa et al. observed[42] that sustained diet-induced weight loss correlated
444 with appreciable adipose transcriptional plasticity and mitochondrial gene expression, where short-
445 term, exercise induced did not. Thus, durations of weight loss, and differences in control diet exposure
446 might reflect the importance of nutritional and exposure factors during weight loss interventions on
447 tissue responses in obesity. Despite not performing profiling of chromatic accessibility, transcriptional
448 factor (TF) binding site enrichment analysis revealed that transcriptional activities of mitochondrial
449 biogenesis factors like Nuclear Respiratory Factor 1 (*Nrf1*) and expression of transcriptional (co)-
450 regulators such as Peroxisome proliferator-activated receptor gamma coactivator 1-alpha (*Ppargc1a*)
451 and *Nrf1*[79] were repressed in obese fat (not shown). As Brandao et al. reported [80] that ablation of
452 DICER1 in adipocytes repressed *Ppargc1a*/*Nrf1*, we can conceive a scenario where reduced DICER1
453 (for instance due to increased *let-7d/e-5p*) drives and/or synergizes with reduced *Ppargc1a*/*Nrf1* levels
454 to impair mitochondrial biogenesis in hypercaloric adipocytes.

455

456 ***Rewiring of embryonal development by gametic miRNAs***

457 In *C. elegans* and *D. melanogaster*, germline gene silencing by small Noncoding RNAs (sncRNA) is
458 well-understood and similar processes are suggested for mammals [19]. miRNAs are not only critical for
459 sperm cell formation [27] and embryogenesis [28], but can also be transferred from sperm to zygotes and it
460 is plausible that oocyte-sperm fusion alters zygotic miRNA pools, affect embryonic development, and
461 instructs phenotypic traits and somatic gene expression in offspring as observed in our intergenerational
462 paradigm. In contrast to DNA-intrinsic epigenetic modifications like DNA methylation (DNAme) and
463 histone post-translational modifications, miRNAs diffuse between and across cellular compartments,
464 are highly abundant in most cells, and, crucially, can be exchanged between cells through extravesicular

465 transport [32]. As mature sperm is transcriptionally inert, and no mechanism exists how sperm senses
466 endocrine information and translates this into differential miRNA levels, sperm relies on 'decoding
467 somatic cell types' that possess these sentinel features and are capable of instructing sperm by transfer
468 of miRNAs and other sncRNAs like mitochondrial tRNA fragments that are exchanged between sperm
469 and oocyte at fertilisation [23]. Furthermore, epididymal cells, somatic epithelial cells of the extragonadal
470 male reproductive tracts, secrete *epididysomes*, microvesicles that fuse with nascent sperm [81], and as
471 we observed several miRNAs concordantly regulated in F_0 adipose tissue and sperm, horizontal miRNA
472 transfer from adipocytes to sperm, potentially via epididysomes is a plausible scenario that still lacks
473 experimental proof in our paradigm. Finally, altering miRNA levels like *miR-199a-5p* in zygotes by
474 microinjection is sufficient to reprogram embryonal metabolism [82], highlighting that miRNA alterations
475 can rewire embryonal development and metabolism which are still compatible with fetal development.

476 **Methods:**

477

478 ***Mice***

479 All animal experiments were approved by the Ministry of Environment and Agriculture Denmark
480 (Miljø- og Fødevarestyrelsen), the license no. 2018-15-0201-01544. All mice were housed under a 12-
481 h light/ 12-h dark cycle in a temperature and humidity-controlled facility and had *ad libitum* access to
482 diets and drinking water. 4-week-old C57BL/6J male mice (Janvier Labs) were fed with a chow diet
483 (NIH-31, Zeigler Brothers Inc., 8% calories from fat) for 2 weeks of acclimatization and then were fed
484 with either a low-fat diet (LF, D12450J, 10% kcal from fat, Research Diet) or a high-fat diet (HF,
485 D12492, 60% kcal from fat, Research Diet) for 9 weeks. After 9 weeks of feeding, half of HF-fed mice
486 were randomly assigned to the diet regression group which was given LFD. LFD is carefully chosen to
487 match food source (animal vs plant) and micronutrient composition of HFD.

488

489 ***Mouse husbandry***

490 All male virgin mice were maintained on the assigned diet until 21 weeks of age and mated with 10-
491 week-old C57BL/6J female virgin mice (Janvier Labs). 8-week-old C57BL/6J female mice were fed
492 with a chow diet for 2 weeks of acclimatization and then were fed with LF during breeding and lactation.
493 Mating was set up for 5 days in a female's cage and vaginal plugs were checked every morning. All
494 mice, including the F_0 HF group, were maintained on LF during breeding to remove confounding effects
495 from maternal diets. Males were sent from breeding cages to the original cage to be fed with the assigned
496 diet for additional 2 weeks and then sacrificed. The offspring from all groups of founders consumed
497 only LF. Representative male offspring from six litters per group were included in all analyses.

498

499 ***Intraperitoneal glucose and insulin tolerance tests:***

500 Mice were fasted for 6 h for glucose-tolerance tests. Fasting glucose levels were measured and then
501 mice were intraperitoneally injected with 2 g/kg body weight of 20 % glucose solution (B. Braun
502 Medical A/S). For intraperitoneal insulin-tolerance tests, random-fed glucose levels were measured,
503 and mice were intraperitoneally injected with 0.75 IU/kg body weight of 100IU stock insulin (Novo

504 Nordisk). Blood glucose levels were measured at 15, 30, 60, 90, and 120 min after injecting glucose or
505 insulin using a CONTOUR®NEXT glucometer (Bayer). For ipGTT/ipITT, we omitted mice with
506 strongly delayed rises in glucose and no discernible drop in blood glucose, respectively, from analyses
507 as this was the consequence of mal injection outside the peritoneum.
508
509 ***Tissue collection:***
510 Mice were sacrificed by carbon dioxide euthanasia. Livers, eWAT, iWAT and BAT were weighed,
511 snap-frozen in liquid nitrogen, and stored in -80 °C. Pieces from liver and eWAT were fixed in 4%
512 paraformaldehyde (PFA) for histology analysis. For serum collection, blood collected by the cardiac
513 puncture was centrifuged at 2,000 g for 15 min. The supernatant was collected and stored in -80 °C.
514
515 ***Sperm collection:***
516 Mature sperm cells were collected from the cauda epididymis. Briefly, sperm cells are allowed to swim
517 out from the cauda epididymis and incubate in PBS at 37 °C for 15 min. Supernatant containing sperms
518 was passed through a 40-µm cell strainer and then incubated in a somatic cell lysis buffer (0.5 % Triton-
519 X and 0.1 % SDS) for 40 min on ice. Sperms were centrifuged at 600 g for 5 min and the pellets were
520 washed with PBS and pelted again at 600 g for 5 min. The supernatant was discarded, and the pellets
521 were snap-frozen in liquid nitrogen and stored at -80 °C.
522
523 ***Zygotic miRNA microinjection and embryo implantation:***
524 Ovulation of prepubescent (4-week-old) C57BL/6J females was induced by intraperitoneal (IP)
525 injection of PMSG, 5 IU/female, followed by IP injection of hCG, 5IU/female, 47h later. After the
526 second injection, females were set in breeding with C57BL/6J stud males. Next morning, they were
527 monitored for formation of a vaginal plug (indicating mating has occurred during the night). Females
528 were euthanized and oviducts were dissected to harvest the cumuli containing zygotes and unfertilized
529 oocytes. Cumuli were disaggregated by incubation in a 10mg/ml solution of Hyaluronidase (Sigma-
530 Aldrich ref. H4272) in M2 medium (Sigma-Aldrich ref. M7167) at RT for 10 minutes. Zygotes were
531 sorted out, assessed by the presence of the second polar body and cultured in KSOM medium (Merck

532 Millipore ref. MR-106-D). Oocytes were discarded. Each miRNA was diluted at 10 ng/ul in
533 microinjection buffer (5 mM Tris, 0.1 mM EDTA, pH 7.4) as stock solution and kept at -80 °C. The
534 day of microinjection, 1,5 ng/ul solutions were prepared from the stock, and injected in the pronuclei
535 of the zygotes following standard microinjection procedures. miRIDIAN mimics were ordered from
536 Dharmacon: Inert miRNA control is based on *C.elegans cel-mir-67* which is not expressed in mouse or
537 human cells (5'-UCACAACCUCCUAGAAAGAGUAGA-3', cat. no. CN-001000-01-05), *mmu-let-*
538 *7d-5p* (cat. no. C-310486-07-0002) and *mmu-let-7e-5p* (cat. no. C-310507-07-0005). Injected zygotes
539 were cultured in KSOM until the microinjection session was completed and then cryopreserved by the
540 "Slow Freezing" Method (Manipulating the Mouse Embryo, a Laboratory Manual, fourth edition,
541 Chapter 16, Richard Behringer et al. Cold Spring Harbor Laboratory Press, 2014) and transported to
542 SDU at -150 °C for embryo transfer and recovery.
543
544 The frozen microinjected embryos were thawed at SDU and cultured in KSOM (Merck, MR-121-D)
545 for 40 minutes (Manipulating the Mouse Embryo, a Laboratory Manual, fourth edition, Chapter 16,
546 Richard Behringer et al. Cold Spring Harbor Laboratory Press, 2014). Viable embryos with intact zona
547 pellucida were selected for further transfer. These embryos were then washed in 10 drops of M2 and
548 surgically transferred to the oviducts of 0.5 dpc pseudo pregnant females. Pseudopregnancy was
549 induced in the females by mating them with a vasectomized male. Prior to implantation, the pseudo
550 pregnant females were anesthetized with ketamine (100 mg/kg) and xylazine (10 mg/kg) through
551 intraperitoneal injection, and the surgical embryo transfer procedure was performed following the
552 protocol described by Behringer et al. (Manipulating the Mouse Embryo, a Laboratory Manual, fourth
553 edition, Chapter 6, Richard Behringer et al. Cold Spring Harbor Laboratory Press, 2014). Postoperative
554 analgesic treatment with carprofen (5 mg/kg) was administered subcutaneously for 48 hours.
555
556 ***8-cell-morula blastomere disaggregation:***
557 miRNAs were injected in the embryo at zygote stage as described above. After injection, embryos were
558 incubated in KSOM (KSOM-Embryomax advanced embryo medium, Merck Millipore #MD-101-D)
559 for 48-56 hours at 37 °C, in 5% $C0_2$. The culture medium was refreshed daily. In the afternoon of the

560 third day of culture, when the embryos had reached the 8-cell morula stage, they were incubated at RT
561 in Tyrod's solution (Sigma-Aldrich T1788) for up to 30 seconds until the zona pellucida was completely
562 dissolved. Afterwards the naked morulae were washed through three drops of M2 medium (Sigma-
563 Aldrich M7167) and finally incubated in KSOM without Ca^{2+} and Mg^{2+} at RT for 20 minutes. Then,
564 embryos were moved to a new drop of fresh M2 medium and there, pipetted up and down repeatedly to
565 facilitate the blastomere disaggregation. When single blastomeres were obtained, they were individually
566 transferred to single wells of a 96-well single-cell-sequencing plate from VWR (Cat. No. 82006-636)
567 with 2 ul of RNAse inhibitor mix (containing 0.12 ul Triton X-100 10 %, 0.1 ul RNAse inhibitor (Takara
568 (Cat. No. 2313B, 40 U/ul), 1.78 ul MilliQ water (RNAse-free)). Plates were them frozen at -80 °C until
569 the sequencing was performed.
570
571 ***Lipidomics and Metabolomics:***
572 ***Serum Extraction:***
573 100 µL of serum was mixed with 1000 µL of a 2:1 chloroform/methanol solution and 200 µL of water.
574 Four blank samples, each containing 100 µL of water, were processed in parallel. The mixtures were
575 shaken at 1000 rpm for 30 minutes at 4°C, followed by centrifugation at 16,000g for 10 minutes at 4
576 °C to separate the phases. The aqueous phase was re-extracted with 350 µL of an 86:14:1
577 chloroform/methanol/water solution. The organic phase from this re-extraction was combined with the
578 corresponding organic phase from the initial extraction. Aqueous fraction was dried using SpeedVac,
579 while the organic phase was dried under a stream of nitrogen. For subsequent analysis, the dried aqueous
580 fractions were reconstituted in 30 µL of 1 % formic acid for metabolomics. The organic phase was
581 reconstituted in 30 µL of lipidomic solvent A (5:1:4 isopropanol/methanol/water with 5 mM ammonium
582 acetate and 0.1 % acetic acid). A pooled quality control sample was prepared for each analytical setup
583 by combining 5 µL from each sample, excluding blanks.
584
585 ***Lipidomic analysis:***
586 For **lipidomic** analysis, 2.5 µL of each sample was injected into an Agilent 1290 Infinity UPLC system
587 (Agilent Technologies, Santa Clara, CA, USA) equipped with a Zorbax Eclipse Plus C18 guard column

588 (2.1 × 5 mm, 1.8 µm) and an analytical column (2.1 × 150 mm, 1.8 µm), maintained at 50 °C. Analytes
589 were eluted at a flow rate of 400 µL/min using eluent A (water with 5 mM ammonium acetate and 0.1
590 % acetic acid) and eluent B (99:1 isopropanol/water with 5 mM ammonium acetate and 0.1 % acetic
591 acid). The gradient was as follows: 0 % B from 0 to 1 min, 0-25 % B from 1 to 1.5 min, 25-95 % B
592 from 1.5 to 12 min, 95 % B from 12 to 14 min, and 95-0 % B from 14 to 15 min, followed by a 3-
593 minute equilibration. For **metabolomics** analysis, 1.5 µL of each sample was injected into the same
594 UPLC-MS system, but with a ZORBAX Eclipse Plus C18 guard column (2.1 × 50 mm, 1.8 µm) and an
595 analytical column (2.1 × 150 mm, 1.8 µm) maintained at 40°C. Eluent A was 0.1 % formic acid, and
596 eluent B was 0.1 % formic acid in acetonitrile. The gradient was as follows: 3 % B from 0 to 1.5 min,
597 3-40 % B from 1.5 to 4.5 min, 40-95 % B from 4.5 to 7.5 min, 9 5% B from 7.5 to 10.1 min, and 95-3
598 % B from 10.1 to 10.5 min, followed by a 3.5-minute equilibration. Both analyses were performed on
599 a 6530B quadrupole time-of-flight mass spectrometer (Agilent Technologies, Santa Clara, CA, USA)
600 for mass spectrometric detection in positive and negative ion modes. MS1 mode settings included a
601 scanning range of 50-1700 m/z for lipidomic and 10-1050 m/z for metabolomics, with 2 scans/sec.
602 Internal calibration was performed using Hexakis (1H,1H,3H-tetrafluoropropoxy) phosphazene
603 delivered through a second needle in the ion source via an isocratic pump running at 20 µL/min. Iterative
604 data-dependent MS2 mode was used for fragmentation in both analyses with the following settings:
605 collision energy at 40 V (lipidomics) and 20-40 V (metabolomics), precursor threshold at 5000 counts,
606 and active exclusion after 2 spectra, with re-inclusion after 0.5 min.
607
608 ***Data Processing and Normalization:***
609 All data was converted. mzML format using ProteoWizard[83]. Lipidomics data was annotated in MS-
610 Dial (v. 4.9) against the incorporated lipid-blast[84] with an MS1/MS2 mass tolerance of 0.005/0.01 Da
611 and a minimum identification score of 70 %. The annotated compounds were exported to PCDL
612 manager B.08.00 (Agilent Technologies) to create a database for area extraction in Profinder 10.0
613 (Agilent Technologies). Metabolomics data was processed in MzMine (v2.59) utilizing modules such
614 as ADAP chromatogram builder and deconvolution. Compounds were annotated at Metabolomics
615 Standards Initiative (MSI) levels 3 using the libraries of National Institute of Standards and Technology

616 2017 (NIST17) and MassBank of North America (MoNa). Features with signals less than 5 times those
617 in blanks or missing in more than 20 % of QC samples were removed and signals were QC corrected
618 using statTarget[85].
619
620 ***Data analysis:***
621 For **metabolomics** pathway enrichment analysis (KEGG pathways of Mus Musculus) comparing F_0 LF
622 and F_0 HF serum (parameters 'Scatter plot', 'Hypergeometric test', 'relative-betweenness Centrality',
623 'Use all compounds in the selected pathway library') of differentially abundant polar metabolites (pV
624 ≤ 0.1) were loaded into Metaboanalyst 6.0. For **lipidomics** and **metabolomics** principal component
625 analysis and heatmap representation of indicated no. of differentially abundant lipids and metabolites
626 were generated using ‚Statistical Feature' (one-factor option), Sample normalization = ‚Normalization
627 by sum', Data transformation = ‚Log transformation (base 10)' and Data scaling = ‚Mean Centering'.
628
629 ***Serum insulin and leptin ELISA:***
630 Serum insulin and leptin levels were measured by mouse insulin ELISA kit (Mercodia, Uppsala,
631 Sweden) and mouse leptin ELISA kit (Crystal Chem, IL, USA) according to manufactures' protocol.
632
633 ***Histology and staining:***
634 Liver and adipose tissues fixed with 4 % of paraformaldehyde were used for histology analyses.
635 Formalin-fixed, paraffin-embedded tissues were cut into 3 µm sections. Sections were stained by
636 haematoxylin and eosin (H&E) and Sirius Red by standard procedures at the Department of Pathology
637 at Odense University Hospital, Odense, Denmark. Immunohistochemistry for CD45 was performed on
638 Ventana BenchMark Ultra (Roche) with ready-to-use CD45 (LCA) (2B11 & PD7/26) Mouse
639 Monoclonal Antibody.
640
641 A liver pathologist (SD) assigned steatosis, lobular inflammation, ballooning, fibrosis stage, and portal
642 inflammation. Steatosis was graded as S0 (< 5% hepatocytes with large fat vacuoles), S1 (5-33%), S2
643 (>33-66%), and S3 (>66% hepatocytes with large fat vacuoles)[86]. Lobular inflammation (0-3) and

644 hepatocellular ballooning (0-2) were assessed according to the NAS-CRN Activity Score by Kleiner et
645 al.[86]. Also, portal inflammation was assessed, using a 4-tiered score by Kleine et al. Liver fibrosis stage
646 was assessed according to NAS-CRN for fibrosis; F-0, no fibrosis; F-1, perisinusoidal or periportal
647 fibrosis; F-2, perisinusoidal and portal/periportal fibrosis; F-3, bridging fibrosis; F-4, cirrhosis.
648
649 ***Measurement of adipocyte volumes:***
650 The volume weighted mean volume of adipocytes was determined from the H&E sections with
651 newCAST stereology software (Visiopharm), autodisector; measurements on systematic, randomly
652 selected fields were performed on by at least 75 adipocyte profiles in each tissue.
653
654 ***Bulk proteomics from epididymal white adipose tissue:***
655 Deep frozen fat pads (200 mg of epididymal adipose tissue) were powdered with mortar-pestle and
656 subjected to homogenization with ceramic beads (Percellys, 5500 rpm, 2 x 10 seconds, 30 seconds
657 break) in the buffer containing 50 mM HEPES pH 7.4, 1 % Triton X-100, 100 mM NaF, 10 mM sodium
658 orthovanadate, 10 mM EDTA, 0.2 % SDS, 100 mM NaCl. Tissue homogenates were further processed
659 to remove the nucleic acid traces (Diagenode SA; 10 min, cycle 30/30 seconds, at 4 °C). Floating fat
660 and tissue debris were removed from protein extracts by centrifugation at 20000 x g. 150 mg of proteins
661 were precipitated with 4x volume of ice-cold acetone and washed with ice-cold acetone twice. Air-dry
662 pellets were resuspended in 8M Urea/50 mM triethylammonium bicarbonate (TAEB) buffer
663 supplemented with a protease inhibitor cocktail (Sigma). 50 mg of the samples were incubated with 5
664 mM dithiothreitol at 25°C for 60 min, followed by treatment with 40 mM chloroacetamide for 30 min
665 (room temperature, light-protected). Lys-C protease (enzyme: substrate ratio of 1:75) was added for 4
666 hours at 25 °C. The TAEB-diluted sample (2M Urea final) was supplemented with trypsin (1:75 ratio)
667 followed by overnight digestion at 25 °C. Acidified peptides (1 % formic acid final) were purified on
668 the SDR-RP (C18) multi-stop-and-go-tip (Stage Tip)[87].
669
670 ***LC MS/MS Label-Free Quantitative Proteomic Analysis from epididymal white adipose tissue:***

671 All samples were analyzed by the Proteomics Facility on a Q Exactive Plus Orbitrap mass spectrometer
672 coupled to an EASY nLC 1000 (Thermo Scientific). Peptides were loaded with solvent A (0.1 % formic
673 acid in water) onto an in-house packed analytical column (50 cm - 75 µm I.D., filled with 2.7 µm
674 Poroshell EC120 C18, Agilent) and separated with 150 min gradients. Peptides were
675 chromatographically separated at a constant flow rate of 250 nL/min using the following gradient: 4-6
676 % solvent B (0.1 % formic acid in 80 % acetonitrile) within 5.0 min, 6-23 % solvent B within 120.0
677 min, 23-54 % solvent B within 7.0 min, 54-85 % solvent B within 6.0 min, followed by washing and
678 column equilibration. The mass spectrometer was operated in data-dependent acquisition mode. The
679 MS1 survey scan was acquired from 300-1750 m/z at a resolution of 70,000. The top 10 most abundant
680 peptides were isolated within a 2.1 Th window and subjected to HCD fragmentation at a normalized
681 collision energy of 27 %. The AGC target was set to 5E5 charges, allowing a maximum injection time
682 of 60 ms. Product ions were detected in the Orbitrap at a resolution of 17,500. Precursors were
683 dynamically excluded for 20.0 s. All mass spectrometric raw data were processed with MaxQuant[88]
684 (version 1.5.3.8, using default parameters and searched against the canonical murine Uniprot reference
685 proteome (UP589, downloaded on 28/08/2020). Label-free quantification option was enabled as was
686 the match-between runs option between replicates. Follow-up analysis was done in Perseus[89] 1.6.15.
687 Hits from the decoy database, the contaminant list, and those only identified by modified peptides were
688 removed. Afterwards, results were filtered for data completeness in replicate groups and LFQ values
689 imputed using sigma downshift with standard settings. Finally, FDR-controlled T-tests between sample
690 groups were performed with s0 = 0.2. Proteins were annotated on GOBP, GOCC, KEGG and Pfam
691 terms. Afterwards, all one-way ANOVA (s= 0.2) significant candidates were Zscored and hierarchically
692 clustered using the Euclidean distance model. Resulting clusters were merged onto the whole data set
693 and a Fisher Exact Test calculated on cluster level with the whole dataset as background.
694
695 ***RNA isolation from mouse tissue and primary adipocytes:***
696 Total RNAs from tissues, sperm, and primary adipocytes were isolated using the TRI reagent (Sigma)
697 followed by clean-up with RPE buffer (Qiagen, Germany). The quality of RNA was validated by the

698 Agilent RNA 6000 Nano-Kit in Agilent 2100 Bioanalyzer according to the manufacturer's protocol.
699 (Agilent Technologies, Waldbronn, Germany).
700
701 ***RNA sequencing:***
702 *Small RNA sequencing:* (1) For sRNA-seq from F_0 sperm, library preparation and sRNA-seq was
703 performed at Cologne Center for Genomics, Germany. 50 ng of total RNA was used for library
704 preparation followed by size selection (Small RNA-Seq Library Prep Kit, Lexogen). The library was
705 sequenced in 1x50-bp single-end reads on NovaSeq6000 serie no. A00316. (2) Small RNA sequencing
706 from F_0 and F_1 eWAT was carried out after quality control, 125 ng of total RNA was used for library
707 preparation (Nextflex library kit) followed by sequencing by 1x50-bp single-end reads on Illumina
708 Novaseq 6000. *mRNA sequencing:* mRNA sequencing was performed in-house. After quality control,
709 1 µg of total RNA was used for library preparation (NEBNext RNA prep kit) followed by 2x50bp
710 paired-end sequencing on Illumina Novaseq 6000.
711
712 ***RNAseq data analysis:***
713 ***Small RNA sequencing of spermatozoa:*** SncRNA-seq analysis of murine sperm was analyzed with
714 Seqpac ver. 1.2.0, where sncRNA biotypes were annotated with 1 mismatch against Ensembl protein
715 and non-coding RNA from GRCm39, miRbase, piRNA from piRBase ver. 3.0, tRNA from tRNAscan-
716 SE, rRNA from RNAcentral and mitochondria from GRCm39:MT. Biotypes were assessed based on
717 the following hierarchy: miRNAs, mitochondrial rRNAs, rRNAs, mitochondrial protein-coding
718 mRNAs, mitochondrial tRNAs, tRNAs, piRNAs, nuclear protein coding mRNAs, lncRNAs, and
719 miscRNAs. Baseline filtering of 1 read per sample and size of 15 to 75 nt long was performed.
720 Normalization was performed with counts per million (cpm).
721
722 ***Small RNA sequencing of somatic (adipose) tissue:***
723 Adapter sequences were trimmed from raw miRNA-seq reads using Cutadapt. The processed reads
724 were mapped to the reference genome and aligned using the Bowtie algorithm within the miRDeep2
725 pipeline [90]. Normalization was performed using the Trimmed Mean of M-values (TMM) method to

726 account for sequencing depth and composition bias. Subsequent data analysis, including differential
727 expression analysis, was conducted in R[91] using respective Bioconductor packages[92].
728
729 ***mRNA sequencing:***
730 Sequencing reads were aligned to the mouse reference genome from Gencode (vM25)[93] using STAR
731 aligner (v 2.7.9a)[94] and gene features were counted by using featureCountsv (2.0.3)[95]. The genes with
732 low expression were filtered out using *filterByExpr* function with default settings from edgeR
733 (v4.0.16)[96] R package. Differential expression analyses were performed using edgeR's *voomLmFit*
734 [97]unction with sample quality weights (sample.weights = TRUE) and linear model "0 + group", whereas
735 group represents the combination of all experimental groups of interest. The experimental conditions
736 and linear models used for each dataset are summarized below. Genes with adjusted p-values below
737 0.05 were considered as differentially expressed. Gene enrichment analyses were performed by
738 clusterProfiler (v4.10.1)[98] R package using both over-representation analysis (ORA) and gene-set
739 enrichment analysis (GSEA) using differentially expressed genes and log-fold-change (logFC) ranked
740 genes ($n_{permutation}$ = 1,000,000), respectively. Gene sets were retrieved from Gene Ontology (GO.db
741 v3.18.0) and Reactome (reactome.db, v1.86.2) databases.
742
743 ***Smart-seq2 mRNA sequencing of murine blastomeres:***
744 Custom-made Smart-seq2 protocol was implemented as before[74]. Briefly, after thawing the plate, 1 µL
745 of dNTP mix (10 mM), 0.1 µL of oligo-dT (100 µM,
746 /5Biosg/AAGCAGTGGTATCAACGCAGAGTAC(T)30VN-3′) and 0.9 ul nuclease-free water was
747 added to each well and the lysis protocol was run when the samples were incubated at 72°C for 3 min
748 in thermocycler. Samples were then put on ice for at least 1 min. Next, 5.60 µL of reverse-transcription
749 mix containing 0.25 µL of RNase I, 2 µL of 5× first-strand buffer, 2 µL of betaine (5 M), 0.06 µL of
750 $MgCl_2$ (1 M), 0.5 µL of DTT (100 mM), 0.5 µL of SuperScript III (200 U/µL), and 0,29 ul of nuclease-
751 free water was added to each well and reverse transcription was carried out as follows: 42 °C-90:00, 42
752 °C-hold, 42 °C—12:20, 10 cycles (50 °C-2:00, 42 °C-2:00), 39 °C-12:00, 70 °C-15:00, 4 °C hold. After
753 the first 90 min of RT, 0.4 µL of 12,5 µM TSO (0.83 µM final concentration) was added to each reaction

754 at room temperature. The plate was resealed, centrifuged for 1 min at 700 g, and placed back on the
755 thermocycler to resume cycling from 42 °C-12:20. After reverse transcription, 15 µL of cDNA
756 enrichment PCR reaction mix containing 12.5 µL of 2× KAPA HiFi HotStart ReadyMix, 0.25 µL of
757 ISPCR primer (10 µM, /5Biosg/AAGCAGTGGTATCAACGCAGAGT-3′), and 2.25 µL of nuclease-
758 free water was added to each well and cDNA enrichment PCR was performed as follows for 21 cycles:
759 98 °C-3:00, 7 cycles (98 °C-0:20, 60 °C-4:00, and 72 °C-6:00), 7 cycles (98 °C-0:20, 64 °C-0:30, and
760 72 °C-6:00), and 7 cycles (98 °C-0:20, 67 °C-0:30, and 72 °C-7:00), 72 °C-10:00, 4 °C-hold. The cDNA
761 purification was performed using AMPure XP beads at a ratio of 1:1 (Beckmann). For elution, Qiagen
762 elution buffer (EB) was used. cDNA concentrations were measured using the Qubit 3.0 fluorometer
763 according to the manufacturer's protocol, and all cDNA samples were analyzed on Agilent Tape station
764 using the High Sensitivity DNA assay.
765
766 Dual-indexed Illumina Nextera XT sequencing libraries were prepared using 25 % of the recommended
767 reaction volumes of Nextera XT components. All Nextera XT libraries were prepared using 125 pg of
768 input cDNA for tagmentation, and were subsequently enriched for 12 PCR cycles, and purified using
769 AMPure XP beads (Beckmann) at a sample:bead ratio of 0.6:1. Library concentrations were measured
770 using Qubit 3.0 fluorometer, and the fragments were analyzed on the Agilent Tape station using the
771 High Sensitivity DNA assay. All libraries were individually normalized and diluted to a concentration
772 of pooled library to 5.4 ng/µL with average size ~515bp (16 nM). The libraries were sequenced on
773 Illumina NextSeq500 in a single-end 75-bp format (FC-404-2005, Illumina). Single-nuclei libraries
774 were sequenced at an average depth of 3 million reads.
775
776 ***Data availability – NGS:***
777 (1) Illumina sRNA-seq and mRNA-seq datasets from F_0 and F_1 liver and eWAT (2) Illumina sRNA-
778 seq from F_0 sperm (3) Illumina mRNA-seq from offsprings sired from of miRNA-injected zygotes (F_m
779 /F_{MI}) eWAT (4) Illumina mRNA-seq from 1° eWA overexpressing *cel-mir-67* (negative control), *let-*
780 *7d-5p* and *let-7e-5p* mimics and (5) Smart-Seq2 single-cell mRNA-seq data from miRNA-injected 8-
781 cell embryos are available as Gene Expression Omnibus (GEO) SuperSeries GSE280278. The data are

available to the reviewers‘ discretion using **url**: https://tinyurl.com/3kdey4sk (**reviewer token**: inqlkwqknhanxsn)

Data availability – Proteomics:

The mass spectrometry proteomics data have been deposited to the ProteomeXchange Consortium via the PRIDE partner repository with the dataset identifier PXD042800. The data are available to the reviewer discretion: Username: reviewer_pxd042800@ebi.ac.uk, Password: QHj9fv33

Data availability – Metabolomics & lipidomics:

All metabolomic and lipidomic datasets are available at the Metabolomics Workbench[99] data repository as project ID PR002238 (https://www.metabolomicsworkbench.org).

Male participants, sperm samples and analysis

The intervention study was approved by the Danish National Committee on Health Research Ethics (SJ-769), the Danish Data Protection Agency (REG-048- 2019) and performed at the Fertility Clinic, Zealand University Hospital, Denmark[77]. The semen samples were collected from obese patients ($\geq$ 30 kg/m2) via masturbation following two days of abstinence. The sperm analyses were performed in the IVF laboratory in an authorized tissue establishment. The other semen samples were diluted with MHM-C (Fujifilm) and frozen immediately for further analysis. The semen samples were collected via masturbation following two days of abstinence, and the samples were analyzed a maximum of two to three hours after production. After liquefaction, ejaculate volume and sperm concentration (total, motile and progressive) were assessed using a microscope (Leica DM750). Sperm concentration was determined with a CellVision counting chamber (CellVision Technology, Heerhugowaard, the Netherlands). Total sperm count was calculated as the product between ejaculate volume and sperm concentration. The sperm analyses were performed in the IVF laboratory in an authorized tissue establishment.

Study design and approvals

810 This prospective intervention study was conducted between May 2020 and April 2022 at the Fertility
811 Clinic, Zealand University Hospital, Denmark. The study was approved by the Danish National
812 Committee on Health Research Ethics (SJ-769), the Danish Data Protection Agency (REG-048- 2019)
813 and registered on the Clinical Trial website (www. ClinicalTrials.gov identifier NCT04721938). All
814 participants provided written informed consent.
815
816 ***Primary adipocyte culture and transfection***
817 Epididymal white adipose tissues (eWAT) from 6- to 8-week-old male C57BL/6J mice were removed,
818 minced, and digested with pre-warmed collagenase media (500 U/mL collagenase type 2 (LS004183,
819 Worthington) and 3.75U/mL DNase I (10104159001, Sigma). Isolated cells were seeded in 6-well
820 plates and grown in DMEM/Ham's F12 medium (21331, Vendor: Gibco), supplemented with 0.1 %
821 Biotin/D-Pantothenate (33 mM/17 mM), 1 % penicillin-streptomycin, and 20 % FBS. Until reaching
822 80 % confluency, primary cells were induced by induction medium with 1 μM rosiglitazone, 850 nM
823 insulin, 1 μM dexamethasone, 250 μM 3-isobutyl-1-methyl-xanthin (IBMX) and 10 % FBS.
824 Subsequently, the medium was changed every other day by a differentiation medium containing 1 μM
825 rosiglitazone, 850 nM insulin and 10 % FBS. 100 nM of Negative Control and *mmu-let-7-d/e-5p* mimics
826 or LNA oligos targeting *Dicer1* were reversely transfected using Lipofectamine RNAiMAX (Thermo
827 Fisher Scientific) at day 4 after induction. Completely differentiated cells were harvested at 7 days after
828 induction for further analysis.
829
830 ***Plasmid design and dual luciferase assay***
831 For the generation of reporter constructs, the specific region of murine *Ago2*, *Dicer-1*, *Hif1an*, *Hk2*,
832 *Cpt2*, *Crat*, *Pcx*, *Idh2*, *Sdha*, *Sdhaf3*, *Pdk2*, *Slc25a22* and *Slc25a24* containing either wildtype (wt) or
833 mutated (mut) *let-7* binding sites was cloned behind the translation stop codon of the firefly-luciferase
834 gene in pmirGLO Dual-Luciferase vector using custom DNA oligos provided by IDT. Renilla luciferase
835 coding in the same plasmid was used as a control reporter for normalization purposes. To report the
836 miRNA activity in mammalian cells, HEK 293 cells were reversely transfected in 96-well plates with
837 60 ng DNA using the TransIT transfection reagent (mirusbio) for 3 days and forwardly transfected with

838 *let-7d/e-5p* mimics for 2 days. HEK-293 cells were cultured in DMEM medium (21013, Gibco)
839 supplemented with 5.6 mM L-glutamine, 1 % penicillin-streptomycin, and 10 % FBS. After 72-h vector
840 transfection and 48-h miRNA mimics transfection, dual luciferase reporter assays (Promega) were
841 performed. The relative activities of firefly luciferase indicating the interaction between miRNA and
842 specific region of targeted mRNA were normalized by the activities of Renilla luciferase.
843
844 ***TaqMan assay and general qPCR***
845 To quantify the levels of mature miRNAs, TaqMan MicroRNA Reverse Transcription Kit (4366596,
846 Thermo Fisher), TaqMan MicroRNA Assays and TaqMan Universal Master Mix II (4440042, Thermo
847 Fisher) were applied according to manufacturer's protocols. Level of mature *hsa-miR-16* was used as
848 internal control in human samples. The relative expression of mature miRNA was calculated using a
849 comparative method (2- ∂∂CT) according to the ABI Relative Quantification Method.
850
851 ***Determination of oxygen consumption rates and measurement of glycolytic activity:***
852 Primary adipocytes from epididymal SVF (1°eWA) were seeded into Agilent Seahorse XFe96
853 Bioanalyzer microplates. Induction and differentiation were performed as described above. After four
854 days of differentiation, 16,000 per well mature adipocytes were re-seeded and transfected with LNA
855 oligos targeting *Dicer1* in DMEM/Ham's F-12 medium plus 10 % Fetal Bovine Serum, 1 % P/S, 0.1 %
856 Biotin and 0.1 % Pantothenic acid (Growth medium) at 37° C and 5 % CO_2. Seahorse measurement
857 was conducted at day 7 from differentiation. For each seahorse plate, the corresponding calibration plate
858 was prepared 24 hours prior to experiments using 200 µl XF Seahorse Calibrant Agilent per well.
859 Corresponding media were prepared before the experiment and consisted of Assay Medium
860 supplemented with 25 mM Glucose, 1 mM Glutamine, 2 mM Sodium Pyruvate, set to pH = 7.4 and
861 filtered sterile. The calibration plate possessed a cartridge having 4 pockets per well. Shortly before the
862 measurement pocket A was filled with 20 µl 20 µM Oligomycin, pocket B with 22 µl 20 µM FCCP and
863 pocket C with 25 µl 5 µM Antimycin A and Rotenone. One hour before measurements, plates were
864 washed with 1x PBS and changed to 180 µl Assay Medium in a non-CO_2 incubator at 37° C. Calibration
865 was started using calibration plates, measuring O_2 and pH LED Value/emission/Initial reference Delta

866 for each well. All measurements started with measuring basal values, followed by injection of
867 Oligomycin, FCCP, and Rotenone plus Antimycin A (MitoStressKit). Measurement parameters were:
868 Mix 3 min, wait 0 min, measure 3 min with each reagent's effect assessed within three consecutive
869 measurement cycles with a total duration of 18 min per reagent injection.
870
871 ***Protein extraction and western blot analysis***
872 After being washed once by phosphate-buffered saline (PBS), the treated cells at harvest time were
873 lysed by RIPA buffer supplemented with cOmplete and PhosSTOP and quantified by Pierce BCA
874 Protein Assay Kit (23227, Thermo Fisher). Western blot analyses were carried out according to standard
875 protocols with primary antibodies against COXIV (Cell Signaling Technologies #4850, 1:1,1000
876 dilution), Cytochrome C (Cell Signaling Technologies #4280, 1:1,1000 dilution), HSP60 (Cell
877 Signaling Technologies #412165, 1:1,1000 dilution), PHB1 (Cell Signaling Technologies #2426,
878 1:1,1000 dilution), pyruvate dehydrogenase (Cell Signaling Technologies #3205, 1:1,1000 dilution),
879 SDHA (Cell Signaling Technologies #11998, 1:1,1000 dilution), SOD1 (Cell Signaling Technologies
880 #4266, 1:1,1000 dilution), VDAC (Cell Signaling Technologies #4661, 1:1,1000 dilution), HK2 (Cell
881 Signaling Technologies #2897, 1:1,1000 dilution), CPT2 (Abcam Ab181114, 1:1,1000 dilution) and
882 IDH2 (Cell Signaling Technologies #60322, 1:1,1000 dilution). Relative protein quantification was
883 normalized by HSC70 (Santa Cruz sc-7298, 1:1000 dilution).
884
885 ***Statistical analysis***
886 Data were shown as mean ± standard error. One-way ANOVA and two-way ANOVA followed by
887 Tukey's multiple comparisons test were used for statistical analysis in *in vivo* experiments. Significant
888 differences between groups were noted in figure legends respectively.
889
890 **Acknowledgements:**
891 We thank the CECAD Proteomics Core Facility for support with proteomics analyses, the Laboratory
892 Manager, Stine Ravn, at The Zealand Fertility Clinic for handling and analysing the sperm samples.
893 We are thankful for technical support from Ronni Nielsen and specialists from the Functional Genomics

and Metabolism NGS team. We wish to thank Bente Møller and Irina Korshuniova from BRIC Single Cell Genomics Core Facility for excellent help for Smart-seq2 experiments. Smart-seq2 work was partly supported by CellX (The Danish Single Cell Examination Platform) funded by the Danish Research Agency through the Danish national research infrastructure program (5229-0009B). JWK, JHP and BDML received funding from the European Research Council Starting Grant TransGenRNA (#675014). JWK, CH, and NS received funding from Sygeforsikring Denmark, University of Southern Denmark and Danish Diabetes Academy that is funded by the Novo Nordisk Foundation (NNF17SA0031406). JWK received support from the NNF Challenge (#33444) and Bioscience and Basic Biomedicine Programs of the NNF (#28416). CH received grants from National Taiwan University (113L7494) and the National Science and Technology, Taiwan (114-2314-B-002-055-). MAM received support from Fundação de Amparo à Pesquisa do Estado de São Paulo (FAPESP) and Conselho Nacional de Desenvolvimento Científico e Tecnológico (CNPq), and Coordenação de Aperfeiçoamento de Pessoal de Nível Superior (CAPES). PK and MRF were supported by the Vetenskapsrådet Consolidator Grant 2022-03953 ‚InSync‘.

908 **Figure legends**

909 **Figure 1: Paternal obesity elicits heritable impairments in glucose metabolism and adipose**
910 **mitochondrial function. (a,b**) Illustration of intergenerational *in vivo* cohorts depicting F_0 groups of
911 **(a)** paternal (F_0) obesity and weight-regression, male and female F_1 offspring mice **(b)** and analytical
912 workflows incl. RNA-seq for mRNA and sRNA, mass spectrometry for protein, and ultra-high pressure
913 liquid chromatography (UPLC) for metabolite and lipid differential regulation in F_0/F_1 epididymal white
914 adipose tissue (eWAT), liver, sperm and serum. **(c)** Body weights of F_0 LF (n=6), F_0 HF (n=13; n=6 for
915 15-24 weeks of age), F_0 HF-LF (n=7, *left*) and F_1 (F_0 LF, n=18), F_1 (F_0 HF, n=25) and F_1 (F_0 HF-LF,
916 n=21, *right*) male C57BL/6N mice. **(d)** Blood glucose during intraperitoneal glucose tolerance test in
917 F_0 LF (n=6), F_0 HF (n=6) and F_0 HF-LF (n=7, *left*) and F_1 (F_0 LF, n=10), F_1 (F_0 HF, n=10) and F_1 (F_0
918 HF-LF, n=10, *right*) male C57BL/6N mice. **(e)** Blood glucose during intraperitoneal insulin tolerance
919 test in F_0 LF (n=6), F_0 HF (n=6) and F_0 HF-LF (n=7, *left*) and F_1 (F_0 LF, n=9), F_1 (F_0 HF, n=10) and F_1
920 (F_0 HF-LF, n=10, *right*) male C57BL/6N mice. **(f)** Relative eWAT weights in F_0 LF (n=6), F_0 HF (n=6)
921 and F_0 HF-LF (n=7, *left*) and F_1 (F_0 LF, n=10), F_1 (F_0 HF, n=10) and F_1 (F_0 HF-LF, n=7, *right*) male
922 C57BL/6N mice. **(g)** Serum leptin levels measured by ELISA in F_0 LF (n=6), F_0 HF (n=6) and F_0 HF-
923 LF (n=7, *left*) and F_1 (F_0 LF, n=8), F_1 (F_0 HF, n=8), and F_1 (F_0 HF-LF, n=8, *right*) male C57BL/6N mice.
924 **(h)** Fractional area size distribution of eWAT adipocytes in **(i)** F_0 LF (n=6), F_0 HF (n=6) and F_0 HF-LF
925 (n=6, *left*) and F_1 (F_0 LF, n=6), F_1 (F_0 HF, n=6) and F_1 (F_0 HF-LF, n=6, *right*) male C57BL/6N mice.
926 **(i,j)** Representative haematoxylin and eosin staining of eWAT of (**i**) F_0 LF, F_0 HF and F_0 HF-LF and **(j)**
927 F_1 (F_0 LF), F_1 (F_0 HF), and F_1 (F_0 HF-LF) male C57BL/6N mice. **(k,l)** Visualisation of high-confidence
928 STRING interaction networks of proteins downregulated in (**k**) F_0 LF (n=6) vs F_0 HF (n=6) and (**l**) F_1
929 (F_0 LF, n=6), F_1 (F_0 HF, n=6) eWAT (*top*) and GOBP enrichment (*bottom*). Two-tailed Student's t-test
930 **(c-e,h)** for each timepoint and adipocyte sizes or one-way ANOVA followed by Tukey's multiple
931 comparisons **(f-h)** were used for statistical analysis. Data are presented as mean ± standard error with
932 individual values shown for n≤10. P-Values are indicated in the panel or represented as letters (**a**,
933 $p<0.05$, F_0 LF versus F_0 HF or F_1 (F_0 LF) versus F_1 (F_0 HF); **b**, $p<0.05$, F_0 HF versus F_0 HF-LF or F_1 (F_0
934 HF) versus F_1 (F_0 HF-LF); **c**, $p<0.05$, F_0 LF versus F_0 HF-LF or F_1 (F_0 LF) versus F_1 (F_0 HF-LF)).

935 **Figure 2: Paternal obesity dysregulates miRNA:mRNA gene networks spurring intergenerational**
936 **mitochondrial dysfunction. (a,b)** Volcano plot of significantly up- (grey) and down-regulated (white)
937 mRNAs in eWAT from **(a)** F_0 HF versus F_0 LF with 3,495 upregulated and 1,639 downregulated
938 mRNAs and (**b**) F_1 (F_0 HF) versus F_1 (F_0 LF) with 1,284 up- and 702 down-regulated mRNAs. Plots
939 show log10 transformed fold-changes (fc) and log10-transformed **(a)** adjusted or **(b)** non-adjusted p-
940 Values of mRNA changes. Mitochondrial complex I-V genes are annotated in the plot. **(c,d)** Gene Set
941 Enrichment Analysis and gene ontology enrichment of biological processes (GOBP) of differentially
942 expressed mRNAs from **(a,b).** GOBP linked to mitochondrial respiration, ATP synthesis and Complex
943 I assembly are marked with blue bars. **(e,f)** Volcano plot of significantly regulated miRNAs in eWAT
944 from **(e)** F_0 HF versus F_0 LF with 154 up- and 193 down-regulated miRNAs and (**f**) F_1 (F_0 HF) versus
945 F_1 (F_0 LF) with 63 up- and 87 downregulated miRNAs. Plots depict log10 transformed fc and log10-
946 transformed p-Values of expression changes. Mitochondria-activating miRNAs are annotated in pink.
947 **(g,h)** STRING interaction networks of **(g)** *miR-378/miR-143* and **(h)** *miR-532-5p* targets predicted by
948 AGO2-CLIP (*left*) and network subset for eWAT proteins downregulated when comparing F_0 LF (n=6)
949 versus F_0 HF (n=6) male C57BL/6N mice. Submodules containing mitochondrial proteins are marked
950 by a red square and proteins marked by red dots are AGO2-CLIP predicted *let-7* targets and
951 downregulated in F0 HF versus F_0 LF eWAT.
952
953 **Figure 3: Obesity reversibly affects sperm sncRNomes and induces *let-7* in eWAT and sperm.**
954 **(a)** Size distribution on nucleotide length of biotypes present in F_0 HF-LF sperm. Data presented is
955 mean cpm per diet. **(b)** Size distribution on nucleotide length of biotypes present in F_0 HF sperm. Data
956 presented is mean cpm per diet. **(c)** Size distribution on nucleotide length of biotypes present in F_0 LF
957 sperm. Data presented is mean cpm per diet. **(d)** Fold change of F_0 HF vs F_0 LF sncRNA in sperm. Each
958 points represents one sequence. **(e)** Fold change of F_0 HF-LF vs F_0 HF sncRNA in sperm. Each points
959 represents one sequence. Dark blue= Mitochondrial tRNA, dark green=piRNA, green=ribosomal RNA,
960 light green =long non-coding RNA, yellow=mitochondrial ribosomal RNA, orange= miRNA, dark
961 orange=protein coding, red= miscellaneous RNA, dark red= tRNA, grey=unannotated. **(f)** Heatmap
962 depicting scaled abundances of miRNAs in F_0 LF, F_0 HF and F_0 HF-LF (n=6/group) eWAT and sperm

963 as determined by sRNA-seq. **(g-i)** Abundance of *miR-143-3p*, *let-7d-5p* and in F_0 LF (n=6), F_0 HF (n=6)
964 and F_0 HF-LF (n=6) eWAT and sperm. One-way ANOVA followed by Tukey's multiple comparisons
965 (g-i) were used for statistical analysis. Data are presented as mean ± standard error with individual
966 values shown for n≤10. P-Values are indicated in the panel.
967
968 **Figure 4: Zygotic delivery of *let-7* causes glucose intolerance in sired F_{MI} mice and impairs**
969 **embryonic mitochondria. (a)** Illustration of experimental workflow for zygotic miRNA injection and
970 phenotypic characterisation of sired offsprings (F_{MI} mice). **(b)** Body weights of male F_{MI} mice sired
971 from with *cel-mir-67* (n=9), *let-7d-5p* (n=14) and *let-7e-5p* (n=14) injected zygotes. **(c,d)** Blood glucose
972 levels **(c)** and glucose AUC **(d)** during intraperitoneal glucose tolerance test in male F_{MI} mice sired from
973 *cel-mir-67cel-mir-67* (n=7), *let-7d-5p* (n=10) and *let-7e-5p* (n=10) injected zygotes. **(e)** Blood glucose
974 levels during intraperitoneal insulin tolerance test in male F_{MI} mice sired from *cel-mir-67* (n=7), *let-7d-*
975 *5p* (n=9) and *let-7e-5p* (n=11) injected zygotes. **(f)** Random-fed blood glucose at indicated in male F_{MI}
976 mice sired from *cel-mir-67* (n=6), *let-7d-5p* (n=6) and *let-7e-5p* (n=6) injected zygotes **(g)** Relative
977 weights of indicated organs from male F_{MI} mice sired from *cel-mir-67* (n=7), *let-7d-5p* (n=6) and *let-*
978 *7e-5p* (n=6) injected zygotes. **(h)** GSEA-GOBP analysis of eWAT of male F_{MI} mice sired from *cel-mir-*
979 *67* (n=5), *let-7d-5p* (n=6) and *let-7e-5p* (n=6) treated zygotes. GOBP linked to mitochondrial
980 respiration, ATP synthesis and Complex I assembly are marked with blue bars. **(i)** Illustration of
981 workflow to obtain single 8-cell stage blastomeres derived from zygotes injected with *cel-mir-67*, *let-*
982 *7d-5p* and *let-7e-5p* subjected to smart-seq2 single-cell sequencing. **(j)** Multidimensional scaling plots
983 of single-cell RNAseq profiles in 8-cell stage blastomeres obtained from *cel-mir-67* (n=22 blastomeres
984 derived from n=3 zygotes), *let-7d-5p* (n=19 cells blastomeres from n=3 zygotes) and *let-7e-5p* (n=20
985 blastomeres derived from n=4 zygotes). **(l,m)** Correlation plot and regression analysis between
986 differential BMI loss (ΔBMI) and expression changes (ΔCt) in human semen (**l**) *LET-7D-5P* and
987 (**m**)*LET-7E-5P.* Two-tailed Student's t-test **(c,e)** per timepoint, one-way ANOVA followed by Tukey's
988 multiple comparisons **(d,g)** or Pearson's regression analysis **(l,m)** were used for statistical analysis. Data
989 are presented as mean ± standard error with individual values shown for n≤10. P-Values are indicated

990 in the panel or represented as letters (**a**, $p<0.05$, *cel-mir-67* versus *let-7d-5p*, **b**, $p<0.05$, *cel-mir-67*
991 versus *let-7e-5p*).
992
993 **Figure 5: Adipocyte *let-7* blunts mitochondrial function via a novel let-7-DICER1 axis**
994 **(a)** Visualisation of high-confidence STRING interaction networks of *let-7* targets predicted by AGO2-
995 CLIP miRNA:mRNA interactions and subsetted for proteins downregulated comparing F_0 LF (n=6)
996 versus F_0 HF (n=6) in eWAT from male C57BL/6N mice. Submodules containing mitochondrial
997 proteins are marked by a red square and proteins marked by red dots are AGO2-CLIP predicted *let-7*
998 targets and downregulated in F0 HF versus F_0 LF eWAT. **(b,c)** Volcano plot of significantly up- (grey)
999 and down-regulated (white) genes in 1°eWA transfected with (**b**) *let-7-d-5p* versus *cel-mir-67*, yielding
1000 974 up- and 1,295 down-regulated genes and (**c**) *let-7-e-5p* versus *cel-mir-67*, yielding 754 up- and 633
1001 down-regulated genes. Genes connected to mitochondrial regulation are marked by blue, genes involved
1002 in miRNA maturation by red dots. **(d)** Relative luciferase activity in HEK293 cells after transfection of
1003 pmirGLO dual luciferase reporter assay (DLRA) constructs harbouring wild-type 3′-UTR or exon
1004 containing *let-7* miRNA responsive elements (MRE) of indicated mitochondrial genes and (**e**) wild-
1005 type and mutated *let-7* MREs in *Dicer1* transfected with 100 nM of *cel-mir-67*, *let-7d-5p* and *let-7d-5p*
1006 mimics. Data represent n≥3 independent biological replicates, each performed in n=3 technical
1007 replicates. **(f-h)** Western blot analysis of 1°eWA transfected with *cel-mir-67*, *let-7d-5p* and *let-7d-5p*
1008 mimics performed using the indicated antibodies detecting **(f)** mitochondrial and **(g)** DICER1 proteins.
1009 HSC70 served as loading control. **(h)** Densitometric quantification of **(f,g)** representing n=3 biological
1010 replicates. **(i)** Western blot (*top*) and quantitative RT-PCR (*bottom*) quantification of DICER1 in
1011 1°eWA transfected using two independent locked nucleic acid (LNA) inhibitors targeting *Dicer1*
1012 mRNA. Data represent n=3 biological replicates, each performed in n=3 technical replicates. **(j,k)**
1013 Oxygen consumption rates (**j,** OCR) and extracellular acidification rates (**k**, ECAR) in 1°eWA
1014 transfected with 100 nM of *negative control LNA*, *Dicer1* LNA1 and *Dicer1* LNA2 and stimulated with
1015 oligomycin (O), FCCP (F) and Antimycin A plus Rotenone (A/R). Experiments are representative of
1016 n≥3 independent biological replicates. **(l)** Western blot analysis of eWAT from F_0 LF (n=4), F_0 HF
1017 (n=4), F_0 HF-LF (n=4) male C57BL/6N mice performed using the indicated antibodies detecting

1018 mitochondrial and DICER1 proteins. HSP90 served as loading control. **(m)** Densitometric
1019 quantification of **(l)** representing n=4 biological replicates. **(n)** Illustration of proposed molecular
1020 mechanism connecting obesity and elevated *let-7* in adipocytes to post-transcriptional silencing of
1021 DICER1 and impaired oxidative phosphorylation and respiration. Two-tailed Student's t-test **(j,k)** for
1022 each timepoint or one-way ANOVA (**d,e,h**) followed by Tukey's multiple comparisons test were used
1023 for statistical analysis. Data are presented as mean ± standard error with individual values shown for
1024 n≤10. P-Values are indicated in the panel or represented as letters (**a**, $p<0.05$, *cel-mir-67* versus *let-7d-*
1025 *5p*; **b**, $p<0.05$, *cel-mir-67* versus *let-7e-5p*).

1026 **Supplementary figure legends:**

1027 **Figure S1: Paternal obesity and weight loss do not affect reproductive fitness and litter sizes. (a)**
1028 Total numbers, number of male and female offsprings, sex ratios and **(b)** litter sizes of pups conceived
1029 by (F_0 LF, n=8), (F_0 HF, n=8) and F_1 (F_0 HF-LF, n=8) bucks.

1030

1031 **Figure S2: Paternal obesity causes heritable alterations in glucose metabolism in male but not in**
1032 **female mice. (a)** Blood glucose area under the curve (AUC) of glucose levels during intraperitoneal
1033 glucose tolerance test in F_0 LF (n=6), F_0 HF (n=6) and F_0 HF-LF (n=7, *left*) mice F_1 (F_0 LF, n=10), F_1
1034 (F_0 HF, n=10) and F_1 (F_0 HF-LF, n=10, *right*) mice. **(b)** Serum insulin levels as measured by ELISA in
1035 F_0 LF (n=6), F_0 HF (n=6) and F_0 HF-LF (n=7, *left*) and F_1 (F_0 LF, n=6), F_1 (F_0 HF, n=8) and F_1 (F_0 HF-
1036 LF, n=8) mice. **(c)** Relative inguinal white adipose tissue (iWAT) weights in F_0 LF (n=6), F_0 HF (n=6)
1037 and F_0 HF-LF (n=7, *left*) and F_1 (F_0 LF, n=10), F_1 (F_0 HF, n=10) and F_1 (F_0 HF-LF, n=7, *right*) mice. **(d)**
1038 Body weights of F_1 (F_0 LF, n=11), F_1 (F_0 HF, n=12) and F_1 (F_0 HF-LF, n=13) female C57BL/6N mice.
1039 **(e)** Blood glucose during intraperitoneal glucose tolerance test in F_1 (F_0 LF, n=8), F_1 (F_0 HF, n=10) and
1040 F_1 (F_0 HF-LF, n=10) female C57BL/6N mice. **(f)** AUC of glucose levels during intraperitoneal glucose
1041 tolerance test in F_1 (F_0 LF, n=8), F_1 (F_0 HF, n=10) and F_1 (F_0 HF-LF, n=10) female C57BL/6N mice. **(g)**
1042 Blood glucose during intraperitoneal insulin tolerance test in F_1 (F_0 LF, n=7), F_1 (F_0 HF, n=9) and F_1 (F_0
1043 HF-LF, n=9) female C57BL/6N mice. **(h)** Random-fed serum glucose levels in F_1 (F_0 LF, n=13), F_1 (F_0
1044 HF, n=12) and F_1 (F_0 HF-LF, n=13) female C57BL/6N mice. (**i)** Relative organ weights in indicated
1045 tissue from F_1 (F_0 LF, n=9), F_1 (F_0 HF, n=10) and F_1 (F_0 HF-LF, n=8) female C57BL/6N mice. Two-
1046 tailed Student's t-test (**d,e**) for individual timepoints or one-way ANOVA followed by Tukey's multiple
1047 comparisons (**a-c,f**) were used for statistical analysis. Data are presented as mean ± standard error with
1048 individual values shown for n≤10. p-Values are indicated in the panel or represented as letters (**a**,
1049 $p<0.05$, F_0 LF versus F_0 HF or F_1 (F_0 LF) versus F_1 (F_0 HF); **b**, $p<0.05$, F_0 HF versus F_0 HF-LF or F_1 (F_0
1050 HF) versus F_1 (F_0 HF-LF); **c**, $p<0.05$, F_0 LF versus F_0 HF-LF or F_1 (F_0 LF) versus F_1 (F_0 HF-LF)).

1051

1052 **Figure S3: Effects of paternal obesity on F_0 and F_1 eWAT proteomes. (a,b)** Visualisation of high-
1053 confidence STRING interaction networks of proteins upregulated in (**a**) F_0 LF (n=6) vs F_0 HF (n=6) and

1054 (**b**) F_1 (F_0 LF, n=6), F_1 (F_0 HF, n=6) eWAT (*top*) and GOBP enrichment of differentially regulated
1055 proteins (*bottom*).
1056
1057 **Figure S4: Paternal obesity elicits alterations in circulating mitochondria-associated metabolites**
1058 **and lipids. (a-c)** Principal component analysis (PCA) representing PC1-2 **(a)** heatmap of the 74 most
1059 differentially regulated serum metabolites **(c)** and (**b**) GOBP term enrichment obtained by integrating
1060 differentially abundant serum metabolites and differentially expressed eWAT genes determined by
1061 RNA-seq in eWAT of F_0 LF versus F_0 HF male C57L/6N mice and integrated using by Metaboanalyst
1062 6.0. (**d,e**) PCA representing PC1-2 **(d)** and heatmap of the 100 most differentially regulated serum lipids
1063 **(e)**. Metabolites and lipids were determined by ultra-performance liquid chromatography in serum of
1064 F_0 LF compared to F_0 HF (n=6 per group) male C57BL/6N mice. **(f-h)** Relative abundances of **(f)**
1065 mitochondrial tricarbon acid intermediates **(g)** mitochondrial Carnitine lipid carriers **(h)** mitochondria-
1066 inactivating short-chain and mitochondria-promoting long-chain ceramides in serum of F_0 LF (n=6), F_0
1067 HF (n=6) and F_0 HF-LF (n=7) mice. One-way ANOVA followed by Tukey's multiple comparisons test
1068 were used for statistical analysis and P vales are indicated in each panel.
1069
1070 **Figure S5: Paternal weight loss corrects obesity-associated mitochondrial dysfunction in eWAT.**
1071 **(a,b)** Volcano plot of significantly up- (grey) and down-regulated (white) mRNAs in eWAT from **(a)**
1072 F_0 HF versus F_0 HF-LF with 2,779 up- and 1,741 down-regulated mRNAs and (**b**) F_1 (F_0 HF) versus F_1
1073 (F_0 HF-F) with 1,118 up- and 550 down-regulated mRNAs. Plots show log10 transformed fold-changes
1074 (fc) and log10-transformed **(a)** adjusted or **(b)** non-adjusted p-Values of mRNA changes. Mitochondrial
1075 complex genes are annotated in the plot. **(c,d)** GSEA and GOBP enrichment of differentially expressed
1076 mRNAs from **(a,b).** Terms linked to mitochondrial respiration, ATP synthesis and Complex I are
1077 marked with blue bars. **(e,f)** Volcano plot of significantly regulated miRNAs in eWAT from **(e)** F_0 HF
1078 versus F_0 HF-F with 147 up- and 148 down-regulated miRNAs and (**f**) F_1 (F_0 HF) versus F_1 (F_0 HF-LF)
1079 with 92 up- and 37 downregulated miRNAs. Plots depict log10 transformed fc and p-Values of mRNA
1080 changes. Mitochondria-activating miRNAs are annotated in pink.
1081

1082 **Figure S6: Paternal obesity does not affect F_1 adipose miRNA expression and meta-inflammation.**
1083 **(a,b)** Multidimensional scaling (MDS) plots and PC1/2 of mRNA changes in eWAT of **(a)** F_0 LF (n=6),
1084 F_0 HF (n=6) and F_0 HF-LF (n=6) and (**b**) F_1 (F_0 HF, n=4), F_1 (F_0 HF, n=6) and F_1 (F_0 HF-LF, n=6) male
1085 C57BL/6N mice determined by mRNA-seq. **(c,d)** Volcano plot of significantly regulated miRNAs in
1086 eWAT from **(c)** F_0 HF versus F_0 LF with 154 up- and 193 down-regulated miRNAs and (**d**) F_1 (F_0 HF)
1087 versus F_1 (F_0 LF) with 62 up- and 87 down-regulated miRNAs. Plots depict log10 transformed fc and
1088 p-Values of mRNA changes. Mitochondria-inactivating miRNAs are annotated in light blue. **(e,f)**
1089 Expression changes reflected by normalised mRNA-seq counts from **(e)** F_0 LF (n=6), F_0 HF (n=6) and
1090 F_0 HF-LF (n=6) and (**f**) F_1 (F_0 HF, n=4), F_1 (F_0 HF, n=5) and F_1 (F_0 HF-LF, n=6) male C57BL/6N mice.
1091 Genes represent markers of classically (M1) or alternatively (M2) activated macrophages/monocytes.
1092 One-way ANOVA followed by Tukey's multiple comparisons (**e,f**) were used for statistical analysis.
1093 Data are presented as mean ± standard error with individual values shown for n≤10.p-Values are
1094 represented as letters (**a**, $p<0.05$, F_0 LF versus F_0 HF or F_1 (F_0 LF) versus F_1 (F_0 HF); **b**, $p<0.05$, F_0 HF
1095 versus F_0 HF-LF or F_1 (F_0 HF) versus F_1 (F_0 HF-LF); **c**, $p<0.05$, F_0 LF versus F_0 HF-LF or F_1 (F_0 LF)
1096 versus F_1 (F_0 HF-LF)).
1097
1098 **Figure S7: Paternal obesity does not affect mitochondrial gene expression in F_0 and F_1 liver. (a,b)**
1099 MDS plots and PC1/2 of mRNA changes in liver of **(a)** F_0 LF (n=6), F_0 HF (n=6) and F_0 HF-LF (n=6)
1100 and (**b**) F_1 (F_0 HF, n=4), F_1 (F_0 HF, n=5) and F_1 (F_0 HF-LF, n=6) male C57BL/6N mice determined by
1101 mRNA-seq. **(c,d)** Volcano plot of significantly up-(grey) and down-regulated (white) genes in liver
1102 from (**c**) F_0 HF versus F_0 LF, 3,312 up- and 1,597 down-regulated genes and (**d**) F_1 (F_0 HF) versus F_1 (F_0
1103 LF), 457 upregulated and 1,041 downregulated genes. Plots depict log10 transformed fold-changes and
1104 log10- transformed **(c)** adjusted or **(d)** non-adjusted p-Values of expression changes. **(e,f)** GSEA and
1105 GOBP enrichment of biological processes expression changes shown in (**c,d**).
1106
1107 **Figure S8: Paternal obesity and weight loss does not affect liver morphology and lipid metabolism**
1108 **in F_1 progeny. (a-f)** Representative **(a,b)** histological (haematoxylin/eosine staining cellular
1109 structures), **(c,d)** fibrosis (Sirius Red staining collagen) and **(e,f)** pan-leukocyte (anti-CD45 stains

1110 leukocytes) stained formalin-fixed paraffine embedded sections in livers of **(a,c,e)** F_0 LF, F_0 HF and F_0
1111 HF-LF and **(b,d,f)** F_1 (F_0 LF), F_1 (F_0 HF) and F_1 (F_0 HF-LF) male C57BL/6N mice. (**g,h**) Pathologist
1112 assessment of macrovesicular and microvesicular steatosis, lobular inflammation and NAS fibrosis
1113 scores in livers of livers of F_0 LF, F_0 HF and F_0 HF-LF as well as in F_1 (F_0 LF), F_1 (F_0 HF) and F_1 (F_0 HF-
1114 LF, n=6 per group). **(i,j)** Expression changes reflected by normalised mRNA-seq counts from F_0 LF
1115 (n=6), F_0 HF (n=6) and F_0 HF-LF (n=6, *left*) and (**f**) F_1 (F_0 HF, n=4), F_1 (F_0 HF, n=5) and F_1 (F_0 HF-LF,
1116 n=5, *right*) male C57BL/6N mice. Data are shown for genes in liver **(i)** lipid and lipoprotein metabolism
1117 and **(j)** mitochondrial beta-oxidation. Data in **(i,j)** are presented as mean ± standard error with individual
1118 values shown for n≤10. p-Values are shown in the panels or represented as letters (**a**, $p<0.05$, F_0 LF
1119 versus F_0 HF or F_1 (F_0 LF) versus F_1 (F_0 HF); **b**, $p<0.05$, F_0 HF versus F_0 HF-LF or F_1 (F_0 HF) versus F_1
1120 (F_0 HF-LF); **c**, $p<0.05$, F_0 LF versus F_0 HF-LF or F_1 (F_0 LF) versus F_1 (F_0 HF-LF)).
1121
1122 **Figure S9: Paternal obesity and weight loss cause only modest changes in spermatozoa**
1123 **mitochondrial tRNA fragments.** Fragments with a mean cpm above 10 shown. **(a)** Sequences mapped
1124 to mitochondrial tRNA, presented as mean cpm per diet. **(b)** Sum cpm per mitochondrial tsRNA
1125 fragment type. Each point represents one sample. (*p<0.05, One-way ANOVA with Tukey's multiple
1126 comparisons). n=6 per diet, pink=F_0 LF, beige= F_0 HF, blue= F_0 HF-LF.
1127
1128 **Figure S10: Zygotic microinjection of obesity associated *let-7* does not affect embryonic viability**
1129 **and implantation.**
1130 Total numbers of zygotes microinjected with *cel-mir-67*, *let-7d-5p* and *let-7e-5p*, total numbers of pups
1131 born and relative survival rates of miRNA-proficient embryos.
1132
1133 **Figure S11: Obesity-associated let-7 impairs adipocyte mitochondrial function via silencing of**
1134 **DICER1.** GSEA-GOBP analysis of differentially abundant mRNAs in 8-cell blastomeres derived from
1135 *cel-mir-67* (n=22), *let-7d-5p* (n=19) and *let-7e-5p* (n=20) injected zygotes (corresponding **Fig.4j**).
1136
1137 **References:**

1 Trerotola, M., Relli, V., Simeone, P. & Alberti, S. Epigenetic inheritance and the missing heritability. *Human genomics* **9**, 17, doi:10.1186/s40246-015-0041-3 (2015).
2 Horsthemke, B. A critical view on transgenerational epigenetic inheritance in humans. *Nature communications* **9**, 2973, doi:10.1038/s41467-018-05445-5 (2018).
3 Bygren, L. O., Kaati, G. & Edvinsson, S. Longevity determined by paternal ancestors' nutrition during their slow growth period. *Acta Biotheor* **49**, 53-59, doi:10.1023/a:1010241825519 (2001).
4 Pembrey, M. E. *et al.* Sex-specific, male-line transgenerational responses in humans. *European journal of human genetics : EJHG* **14**, 159-166, doi:10.1038/sj.ejhg.5201538 (2006).
5 Lumey, L. H., Stein, A. D., Kahn, H. S. & Romijn, J. A. Lipid profiles in middle-aged men and women after famine exposure during gestation: the Dutch Hunger Winter Families Study. *Am J Clin Nutr* **89**, 1737-1743, doi:10.3945/ajcn.2008.27038 (2009).
6 Carone, B. R. *et al.* Paternally induced transgenerational environmental reprogramming of metabolic gene expression in mammals. *Cell* **143**, 1084-1096, doi:10.1016/j.cell.2010.12.008 (2010).
7 Ng, S. F. *et al.* Paternal high-fat diet consumption induces common changes in the transcriptomes of retroperitoneal adipose and pancreatic islet tissues in female rat offspring. *FASEB journal : official publication of the Federation of American Societies for Experimental Biology* **28**, 1830-1841, doi:10.1096/fj.13-244046 (2014).
8 de Castro Barbosa, T. *et al.* High-fat diet reprograms the epigenome of rat spermatozoa and transgenerationally affects metabolism of the offspring. *Molecular metabolism* **5**, 184-197, doi:10.1016/j.molmet.2015.12.002 (2016).
9 de Castro Barbosa, T., Alm, P. S., Krook, A., Barres, R. & Zierath, J. R. Paternal high-fat diet transgenerationally impacts hepatic immunometabolism. *FASEB journal : official publication of the Federation of American Societies for Experimental Biology* **33**, 6269-6280, doi:10.1096/fj.201801879RR (2019).
10 Wang, Y. *et al.* Sperm microRNAs confer depression susceptibility to offspring. *Sci Adv* **7**, doi:10.1126/sciadv.abd7605 (2021).
11 Dias, B. G. & Ressler, K. J. Parental olfactory experience influences behavior and neural structure in subsequent generations. *Nature neuroscience* **17**, 89-96, doi:10.1038/nn.3594 (2014).
12 Gapp, K. *et al.* Implication of sperm RNAs in transgenerational inheritance of the effects of early trauma in mice. *Nature neuroscience* **17**, 667-669, doi:10.1038/nn.3695 (2014).
13 Sun, W. *et al.* Cold-induced epigenetic programming of the sperm enhances brown adipose tissue activity in the offspring. *Nature medicine* **24**, 1372-1383, doi:10.1038/s41591-018-0102-y (2018).
14 Skvortsova, K., Iovino, N. & Bogdanovic, O. Functions and mechanisms of epigenetic inheritance in animals. *Nature reviews. Molecular cell biology* **19**, 774-790, doi:10.1038/s41580-018-0074-2 (2018).
15 Rechavi, O., Minevich, G. & Hobert, O. Transgenerational inheritance of an acquired small RNA-based antiviral response in C. elegans. *Cell* **147**, 1248-1256, doi:10.1016/j.cell.2011.10.042 (2011).
16 Fire, A. *et al.* Potent and specific genetic interference by double-stranded RNA in Caenorhabditis elegans. *Nature* **391**, 806-811, doi:10.1038/35888 (1998).
17 Ashe, A. *et al.* piRNAs can trigger a multigenerational epigenetic memory in the germline of C. elegans. *Cell* **150**, 88-99, doi:10.1016/j.cell.2012.06.018 (2012).
18 de Vanssay, A. *et al.* Paramutation in Drosophila linked to emergence of a piRNA-producing locus. *Nature* **490**, 112-115, doi:10.1038/nature11416 (2012).
19 Rassoulzadegan, M. *et al.* RNA-mediated non-mendelian inheritance of an epigenetic change in the mouse. *Nature* **441**, 469-474, doi:10.1038/nature04674 (2006).

1192 20 Gross, N., Kropp, J. & Khatib, H. MicroRNA Signaling in Embryo Development.
1193 *Biology (Basel)* **6**, doi:10.3390/biology6030034 (2017).
1194 21 Sharma, U. *et al.* Small RNAs Are Trafficked from the Epididymis to Developing
1195 Mammalian Sperm. *Developmental cell* **46**, 481-494 e486,
1196 doi:10.1016/j.devcel.2018.06.023 (2018).
1197 22 Natt, D. *et al.* Human sperm displays rapid responses to diet. *PLoS Biol* **17**,
1198 e3000559, doi:10.1371/journal.pbio.3000559 (2019).
1199 23 Tomar, A. *et al.* Epigenetic inheritance of diet-induced and sperm-borne
1200 mitochondrial RNAs. *Nature* **630**, 720-727, doi:10.1038/s41586-024-07472-3 (2024).
1201 24 Grandjean, V. *et al.* RNA-mediated paternal heredity of diet-induced obesity and
1202 metabolic disorders. *Scientific reports* **5**, 18193, doi:10.1038/srep18193 (2015).
1203 25 Rodgers, A. B., Morgan, C. P., Leu, N. A. & Bale, T. L. Transgenerational epigenetic
1204 programming via sperm microRNA recapitulates effects of paternal stress.
1205 *Proceedings of the National Academy of Sciences of the United States of America*
1206 **112**, 13699-13704, doi:10.1073/pnas.1508347112 (2015).
1207 26 Sharma, U. *et al.* Biogenesis and function of tRNA fragments during sperm
1208 maturation and fertilization in mammals. *Science*, doi:10.1126/science.aad6780
1209 (2015).
1210 27 Korhonen, H. M. *et al.* Dicer is required for haploid male germ cell differentiation in
1211 mice. *PloS one* **6**, e24821, doi:10.1371/journal.pone.0024821 (2011).
1212 28 Bernstein, E. *et al.* Dicer is essential for mouse development. *Nature genetics* **35**,
1213 215-217, doi:10.1038/ng1253 (2003).
1214 29 Chen, Q. *et al.* Sperm tsRNAs contribute to intergenerational inheritance of an
1215 acquired metabolic disorder. *Science*, doi:10.1126/science.aad7977 (2015).
1216 30 Rodgers, A. B., Morgan, C. P., Bronson, S. L., Revello, S. & Bale, T. L. Paternal
1217 stress exposure alters sperm microRNA content and reprograms offspring HPA
1218 stress axis regulation. *The Journal of neuroscience : the official journal of the Society*
1219 *for Neuroscience* **33**, 9003-9012, doi:10.1523/JNEUROSCI.0914-13.2013 (2013).
1220 31 Cropley, J. E., Suter, C. M., Beckman, K. B. & Martin, D. I. Germ-line epigenetic
1221 modification of the murine A vy allele by nutritional supplementation. *Proceedings of*
1222 *the National Academy of Sciences of the United States of America* **103**, 17308-
1223 17312, doi:10.1073/pnas.0607090103 (2006).
1224 32 Zhang, Y., Shi, J., Rassoulzadegan, M., Tuorto, F. & Chen, Q. Sperm RNA code
1225 programmes the metabolic health of offspring. *Nature reviews. Endocrinology* **15**,
1226 489-498, doi:10.1038/s41574-019-0226-2 (2019).
1227 33 Sun, K., Kusminski, C. M. & Scherer, P. E. Adipose tissue remodeling and obesity.
1228 *The Journal of clinical investigation* **121**, 2094-2101, doi:10.1172/JCI45887 (2011).
1229 34 Scherer, P. E. Adipose tissue: from lipid storage compartment to endocrine organ.
1230 *Diabetes* **55**, 1537-1545, doi:10.2337/db06-0263 (2006).
1231 35 Lee, J. H. *et al.* The Role of Adipose Tissue Mitochondria: Regulation of
1232 Mitochondrial Function for the Treatment of Metabolic Diseases. *Int J Mol Sci* **20**,
1233 doi:10.3390/ijms20194924 (2019).
1234 36 Czech, M. P. Mechanisms of insulin resistance related to white, beige, and brown
1235 adipocytes. *Molecular metabolism* **34**, 27-42, doi:10.1016/j.molmet.2019.12.014
1236 (2020).
1237 37 Kahn, C. R., Wang, G. & Lee, K. Y. Altered adipose tissue and adipocyte function in
1238 the pathogenesis of metabolic syndrome. *The Journal of clinical investigation* **129**,
1239 3990-4000, doi:10.1172/JCI129187 (2019).
1240 38 Bartelt, A. & Heeren, J. Adipose tissue browning and metabolic health. *Nature*
1241 *reviews. Endocrinology* **10**, 24-36, doi:10.1038/nrendo.2013.204 (2014).
1242 39 Schottl, T., Kappler, L., Braun, K., Fromme, T. & Klingenspor, M. Limited
1243 mitochondrial capacity of visceral versus subcutaneous white adipocytes in male
1244 C57BL/6N mice. *Endocrinology* **156**, 923-933, doi:10.1210/en.2014-1689 (2015).

40 Heinonen, S., Jokinen, R., Rissanen, A. & Pietilainen, K. H. White adipose tissue mitochondrial metabolism in health and in obesity. *Obes Rev* **21**, e12958, doi:10.1111/obr.12958 (2020).
41 Kusminski, C. M. *et al.* MitoNEET-driven alterations in adipocyte mitochondrial activity reveal a crucial adaptive process that preserves insulin sensitivity in obesity. *Nature medicine* **18**, 1539-1549, doi:10.1038/nm.2899 (2012).
42 Gonzalez-Franquesa, A. *et al.* Remission of obesity and insulin resistance is not sufficient to restore mitochondrial homeostasis in visceral adipose tissue. *Redox Biol* **54**, 102353, doi:10.1016/j.redox.2022.102353 (2022).
43 Schottl, T., Kappler, L., Fromme, T. & Klingenspor, M. Limited OXPHOS capacity in white adipocytes is a hallmark of obesity in laboratory mice irrespective of the glucose tolerance status. *Molecular metabolism* **4**, 631-642, doi:10.1016/j.molmet.2015.07.001 (2015).
44 Soro-Arnaiz, I. *et al.* Role of Mitochondrial Complex IV in Age-Dependent Obesity. *Cell reports* **16**, 2991-3002, doi:10.1016/j.celrep.2016.08.041 (2016).
45 Wang, Y. *et al.* Metformin Improves Mitochondrial Respiratory Activity through Activation of AMPK. *Cell reports* **29**, 1511-1523 e1515, doi:10.1016/j.celrep.2019.09.070 (2019).
46 Borralho, P. M., Rodrigues, C. M. & Steer, C. J. microRNAs in Mitochondria: An Unexplored Niche. *Adv Exp Med Biol* **887**, 31-51, doi:10.1007/978-3-319-22380-3_3 (2015).
47 Bandiera, S. *et al.* Nuclear outsourcing of RNA interference components to human mitochondria. *PloS one* **6**, e20746, doi:10.1371/journal.pone.0020746 (2011).
48 Barrey, E. *et al.* Pre-microRNA and mature microRNA in human mitochondria. *PloS one* **6**, e20220, doi:10.1371/journal.pone.0020220 (2011).
49 Mori, M. A. *et al.* Role of MicroRNA Processing in Adipose Tissue in Stress Defense and Longevity. *Cell metabolism* **16**, 336-347, doi:S1550-4131(12)00322-1 [pii] 10.1016/j.cmet.2012.07.017 (2012).
50 Mori, M. A. *et al.* Altered miRNA processing disrupts brown/white adipocyte determination and associates with lipodystrophy. *The Journal of clinical investigation* **124**, 3339-3351, doi:10.1172/JCI73468 (2014).
51 Oliverio, M. *et al.* Dicer1-miR-328-Bace1 signalling controls brown adipose tissue differentiation and function. *Nature cell biology* **18**, 328-336, doi:10.1038/ncb3316 (2016).
52 Huypens, P. *et al.* Epigenetic germline inheritance of diet-induced obesity and insulin resistance. *Nature genetics* **48**, 497-499, doi:10.1038/ng.3527 (2016).
53 Turpin, S. M. *et al.* Obesity-induced CerS6-dependent C16:0 ceramide production promotes weight gain and glucose intolerance. *Cell metabolism* **20**, 678-686, doi:10.1016/j.cmet.2014.08.002 (2014).
54 Hammerschmidt, P. *et al.* CerS6-dependent ceramide synthesis in hypothalamic neurons promotes ER/mitochondrial stress and impairs glucose homeostasis in obese mice. *Nature communications* **14**, 7824, doi:10.1038/s41467-023-42595-7 (2023).
55 Cui, Q., Yu, Z., Purisima, E. O. & Wang, E. Principles of microRNA regulation of a human cellular signaling network. *Mol Syst Biol* **2**, 46, doi:10.1038/msb4100089 (2006).
56 Hong, H. *et al.* MicroRNA-143 promotes cardiac ischemia-mediated mitochondrial impairment by the inhibition of protein kinase Cepsilon. *Basic Res Cardiol* **112**, 60, doi:10.1007/s00395-017-0649-7 (2017).
57 Das, S. *et al.* miR-181c regulates the mitochondrial genome, bioenergetics, and propensity for heart failure in vivo. *PloS one* **9**, e96820, doi:10.1371/journal.pone.0096820 (2014).
58 Roman, B. *et al.* Nuclear-mitochondrial communication involving miR-181c plays an important role in cardiac dysfunction during obesity. *J Mol Cell Cardiol* **144**, 87-96, doi:10.1016/j.yjmcc.2020.05.009 (2020).

1300 59 Alhadidi, Q. M. *et al.* MiR-182 Inhibition Protects Against Experimental Stroke in vivo
1301 and Mitigates Astrocyte Injury and Inflammation in vitro via Modulation of Cortactin
1302 Activity. *Neurochemical research* **47**, 3682-3696, doi:10.1007/s11064-022-03718-6
1303 (2022).
1304 60 Lee, H. *et al.* microRNA-200a-3p enhances mitochondrial elongation by targeting
1305 mitochondrial fission factor. *BMB reports* **50**, 214-219,
1306 doi:10.5483/bmbrep.2017.50.4.006 (2017).
1307 61 Carrer, M. *et al.* Control of mitochondrial metabolism and systemic energy
1308 homeostasis by microRNAs 378 and 378. *Proceedings of the National Academy of*
1309 *Sciences of the United States of America* **109**, 15330-15335, doi:1207605109 [pii]
1310 10.1073/pnas.1207605109 (2012).
1311 62 Wang, J. X. *et al.* MicroRNA-532-3p regulates mitochondrial fission through targeting
1312 apoptosis repressor with caspase recruitment domain in doxorubicin cardiotoxicity.
1313 *Cell Death Dis* **6**, e1677, doi:10.1038/cddis.2015.41 (2015).
1314 63 Subramanian, A. *et al.* Gene set enrichment analysis: a knowledge-based approach
1315 for interpreting genome-wide expression profiles. *Proceedings of the National*
1316 *Academy of Sciences of the United States of America* **102**, 15545-15550,
1317 doi:0506580102 [pii]
1318 10.1073/pnas.0506580102 (2005).
1319 64 Madsen, S. *et al.* Rapid downregulation of DICER is a hallmark of adipose tissue
1320 upon high-fat diet feeding. *Molecular and cellular endocrinology* **595**, 112413,
1321 doi:10.1016/j.mce.2024.112413 (2025).
1322 65 Brieno-Enriquez, M. A. *et al.* Exposure to endocrine disruptor induces
1323 transgenerational epigenetic deregulation of microRNAs in primordial germ cells.
1324 *PloS one* **10**, e0124296, doi:10.1371/journal.pone.0124296 (2015).
1325 66 Zhu, H. *et al.* The Lin28/let-7 axis regulates glucose metabolism. *Cell* **147**, 81-94,
1326 doi:10.1016/j.cell.2011.08.033 (2011).
1327 67 Frost, R. J. & Olson, E. N. Control of glucose homeostasis and insulin sensitivity by
1328 the Let-7 family of microRNAs. *Proceedings of the National Academy of Sciences of*
1329 *the United States of America* **108**, 21075-21080, doi:10.1073/pnas.1118922109
1330 (2011).
1331 68 Fullston, T. *et al.* Paternal obesity initiates metabolic disturbances in two generations
1332 of mice with incomplete penetrance to the F2 generation and alters the transcriptional
1333 profile of testis and sperm microRNA content. *FASEB journal : official publication of*
1334 *the Federation of American Societies for Experimental Biology* **27**, 4226-4243,
1335 doi:10.1096/fj.12-224048 (2013).
1336 69 Cheong, A. W. *et al.* MicroRNA Let-7a and dicer are important in the activation and
1337 implantation of delayed implanting mouse embryos. *Human reproduction* **29**, 750-
1338 762, doi:10.1093/humrep/det462 (2014).
1339 70 Liu, W. *et al.* Expression of microRNA let-7 in cleavage embryos modulates cell fate
1340 determination and formation of mouse blastocystsdagger. *Biol Reprod* **107**, 1452-
1341 1463, doi:10.1093/biolre/ioac181 (2022).
1342 71 Kolenda, T., Przybyla, W., Teresiak, A., Mackiewicz, A. & Lamperska, K. M. The
1343 mystery of let-7d - a small RNA with great power. *Contemp Oncol (Pozn)* **18**, 293-
1344 301, doi:10.5114/wo.2014.44467 (2014).
1345 72 Yuan, S. *et al.* Sperm-borne miRNAs and endo-siRNAs are important for fertilization
1346 and preimplantation embryonic development. *Development* **143**, 635-647,
1347 doi:10.1242/dev.131755 (2016).
1348 73 Suh, N. & Blelloch, R. Small RNAs in early mammalian development: from gametes
1349 to gastrulation. *Development* **138**, 1653-1661, doi:10.1242/dev.056234 (2011).
1350 74 Pfisterer, U. *et al.* Identification of epilepsy-associated neuronal subtypes and gene
1351 expression underlying epileptogenesis. *Nature communications* **11**, 5038,
1352 doi:10.1038/s41467-020-18752-7 (2020).

75 Tobi, E. W. *et al.* DNA methylation signatures link prenatal famine exposure to growth and metabolism. *Nature communications* **5**, 5592, doi:10.1038/ncomms6592 (2014).
76 Schulz, L. C. The Dutch Hunger Winter and the developmental origins of health and disease. *Proceedings of the National Academy of Sciences of the United States of America* **107**, 16757-16758, doi:10.1073/pnas.1012911107 (2010).
77 Jepsen, I. E. *et al.* Turning waiting time into treatment time: Weight reduction by a lifestyle intervention programme for patients with obesity before fertility treatment. *Reproductive, Female and Child Health* **2**, 133-142, doi:https://doi.org/10.1002/rfc2.46 (2023).
78 Giroud, M. *et al.* Let-7i-5p represses brite adipocyte function in mice and humans. *Scientific reports* **6**, 28613, doi:10.1038/srep28613 (2016).
79 Popov, L. D. Mitochondrial biogenesis: An update. *J Cell Mol Med* **24**, 4892-4899, doi:10.1111/jcmm.15194 (2020).
80 Brandao, B. B. *et al.* Dynamic changes in DICER levels in adipose tissue control metabolic adaptations to exercise. *Proceedings of the National Academy of Sciences of the United States of America* **117**, 23932-23941, doi:10.1073/pnas.2011243117 (2020).
81 Sullivan, R. & Saez, F. Epididymosomes, prostasomes, and liposomes: their roles in mammalian male reproductive physiology. *Reproduction* **146**, R21-35, doi:10.1530/REP-13-0058 (2013).
82 Tan, K. *et al.* Downregulation of miR-199a-5p Disrupts the Developmental Potential of In Vitro-Fertilized Mouse Blastocysts. *Biol Reprod* **95**, 54, doi:10.1095/biolreprod.116.141051 (2016).
83 Chambers, M. C. *et al.* A cross-platform toolkit for mass spectrometry and proteomics. *Nature biotechnology* **30**, 918-920, doi:10.1038/nbt.2377 (2012).
84 Kind, T. *et al.* LipidBlast in silico tandem mass spectrometry database for lipid identification. *Nature methods* **10**, 755-758, doi:10.1038/nmeth.2551 (2013).
85 Luan, H., Ji, F., Chen, Y. & Cai, Z. statTarget: A streamlined tool for signal drift correction and interpretations of quantitative mass spectrometry-based omics data. *Anal Chim Acta* **1036**, 66-72, doi:10.1016/j.aca.2018.08.002 (2018).
86 Kleiner, D. E. *et al.* Design and validation of a histological scoring system for nonalcoholic fatty liver disease. *Hepatology* **41**, 1313-1321, doi:10.1002/hep.20701 (2005).
87 Rappsilber, J. & Mann, M. Analysis of the topology of protein complexes using cross-linking and mass spectrometry. *CSH Protoc* **2007**, pdb prot4594, doi:10.1101/pdb.prot4594 (2007).
88 Tyanova, S., Mann, M. & Cox, J. MaxQuant for in-depth analysis of large SILAC datasets. *Methods in molecular biology* **1188**, 351-364, doi:10.1007/978-1-4939-1142-4_24 (2014).
89 Tyanova, S. *et al.* The Perseus computational platform for comprehensive analysis of (prote)omics data. *Nature methods* **13**, 731-740, doi:10.1038/nmeth.3901 (2016).
90 Friedlander, M. R., Mackowiak, S. D., Li, N., Chen, W. & Rajewsky, N. miRDeep2 accurately identifies known and hundreds of novel microRNA genes in seven animal clades. *Nucleic acids research* **40**, 37-52, doi:10.1093/nar/gkr688 (2012).
91 Chan, B. K. C. Data Analysis Using R Programming. *Adv Exp Med Biol* **1082**, 47-122, doi:10.1007/978-3-319-93791-5_2 (2018).
92 Reimers, M. & Carey, V. J. Bioconductor: an open source framework for bioinformatics and computational biology. *Methods Enzymol* **411**, 119-134, doi:10.1016/S0076-6879(06)11008-3 (2006).
93 Frankish, A. *et al.* GENCODE reference annotation for the human and mouse genomes. *Nucleic acids research* **47**, D766-D773, doi:10.1093/nar/gky955 (2019).
94 Dobin, A. *et al.* STAR: ultrafast universal RNA-seq aligner. *Bioinformatics* **29**, 15-21, doi:10.1093/bioinformatics/bts635 (2013).

95 Liao, Y., Smyth, G. K. & Shi, W. featureCounts: an efficient general purpose program for assigning sequence reads to genomic features. *Bioinformatics* **30**, 923-930, doi:10.1093/bioinformatics/btt656 (2014).

96 Robinson, M. D., McCarthy, D. J. & Smyth, G. K. edgeR: a Bioconductor package for differential expression analysis of digital gene expression data. *Bioinformatics* **26**, 139-140, doi:10.1093/bioinformatics/btp616 (2010).

97 Law, C. W., Chen, Y., Shi, W. & Smyth, G. K. voom: Precision weights unlock linear model analysis tools for RNA-seq read counts. *Genome biology* **15**, R29, doi:10.1186/gb-2014-15-2-r29 (2014).

98 Wu, T. *et al.* clusterProfiler 4.0: A universal enrichment tool for interpreting omics data. *Innovation (Camb)* **2**, 100141, doi:10.1016/j.xinn.2021.100141 (2021).

99 Sud, M. *et al.* Metabolomics Workbench: An international repository for metabolomics data and metadata, metabolite standards, protocols, tutorials and training, and analysis tools. *Nucleic acids research* **44**, D463-470, doi:10.1093/nar/gkv1042 (2016).

Figure 1: Paternal obesity elicits heritable impairments in glucose metabolism and adipose mitochondrial function

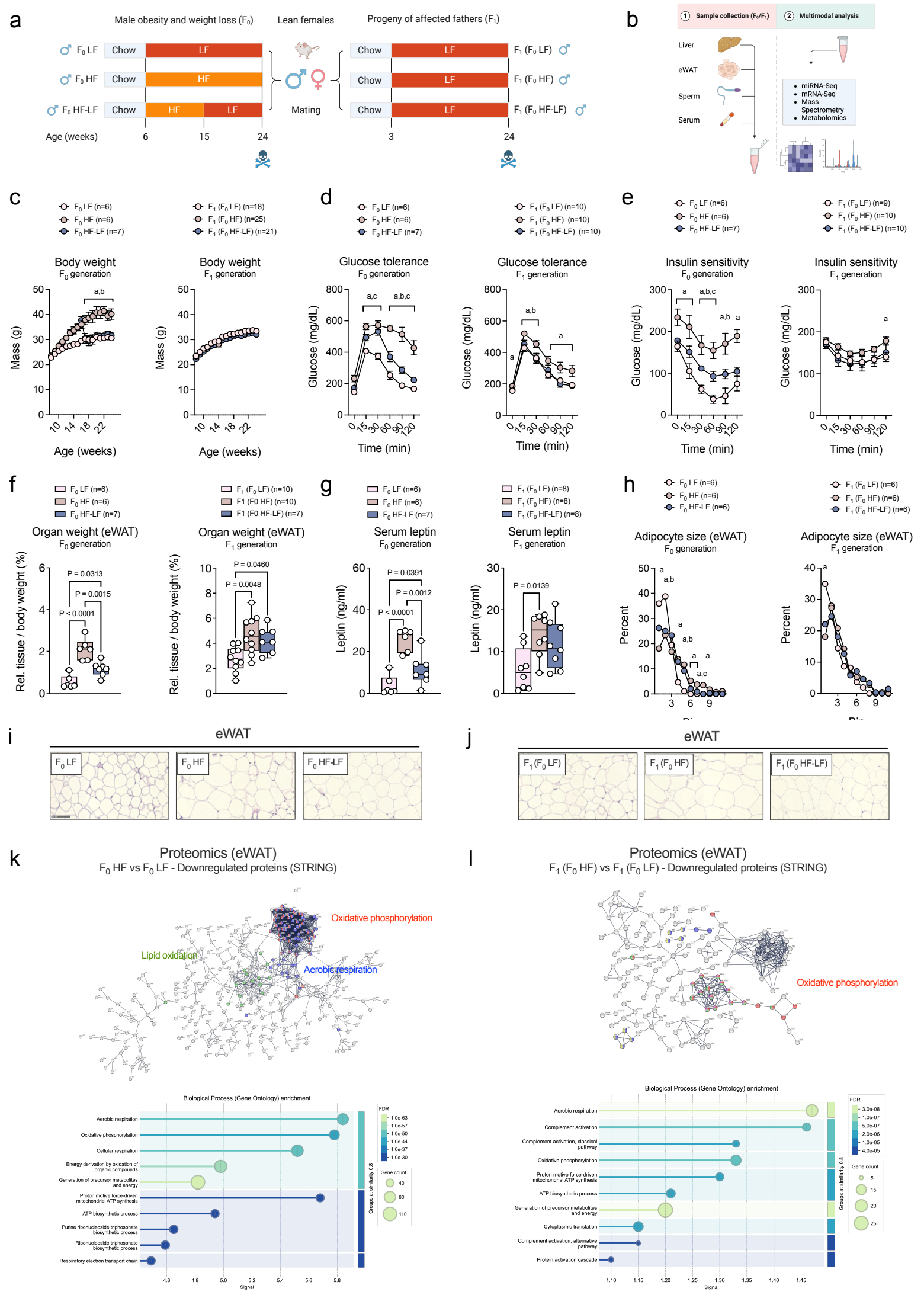

Figure 2: Paternal obesity dysregulates miRNA:mRNA gene networks spurring intergenerational mitochondrial dysfunction

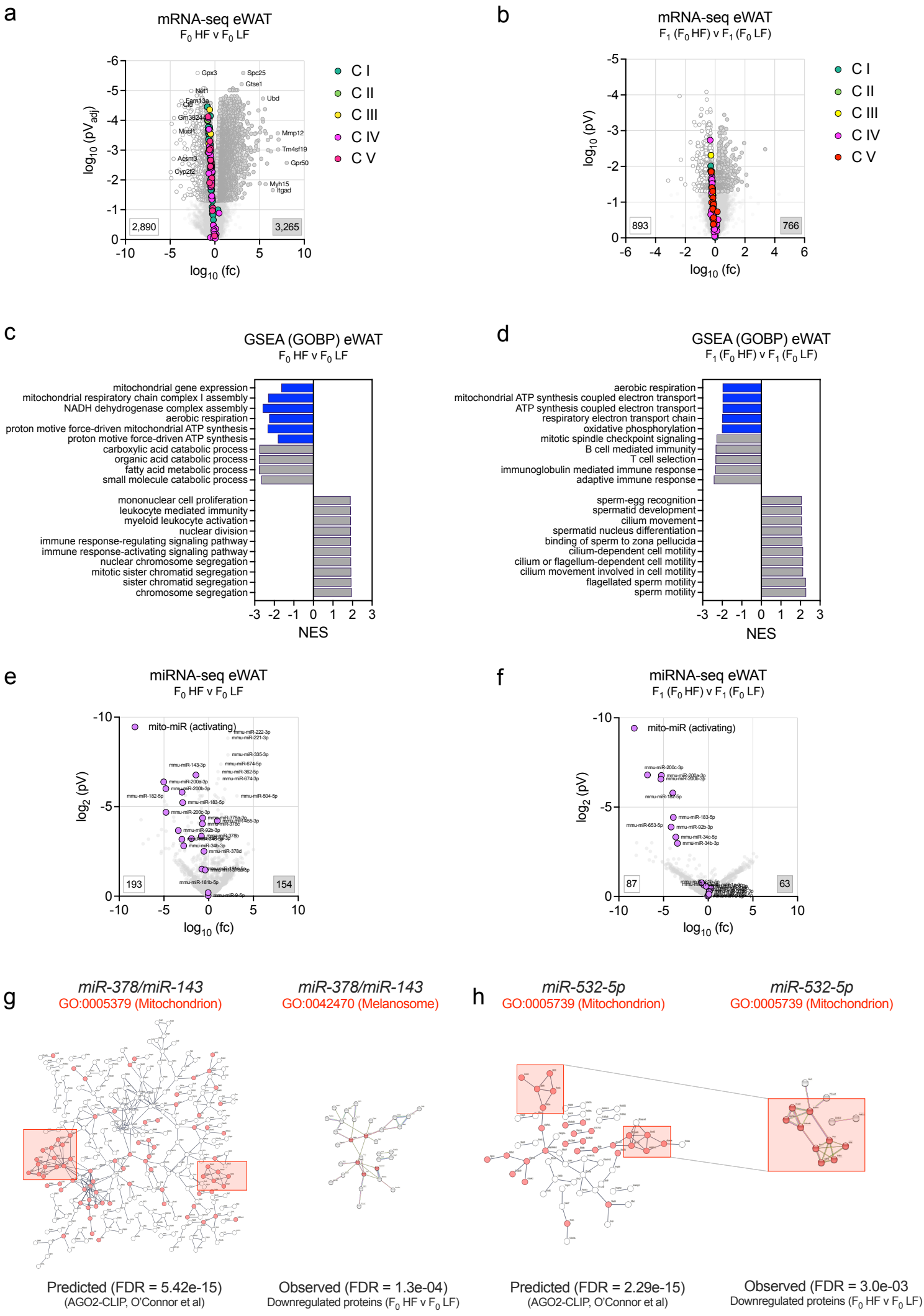

Figure 3: Paternal obesity reversibly affects sperm sncRNomes and induces *let7 isoforms* in eWAT and sperm.

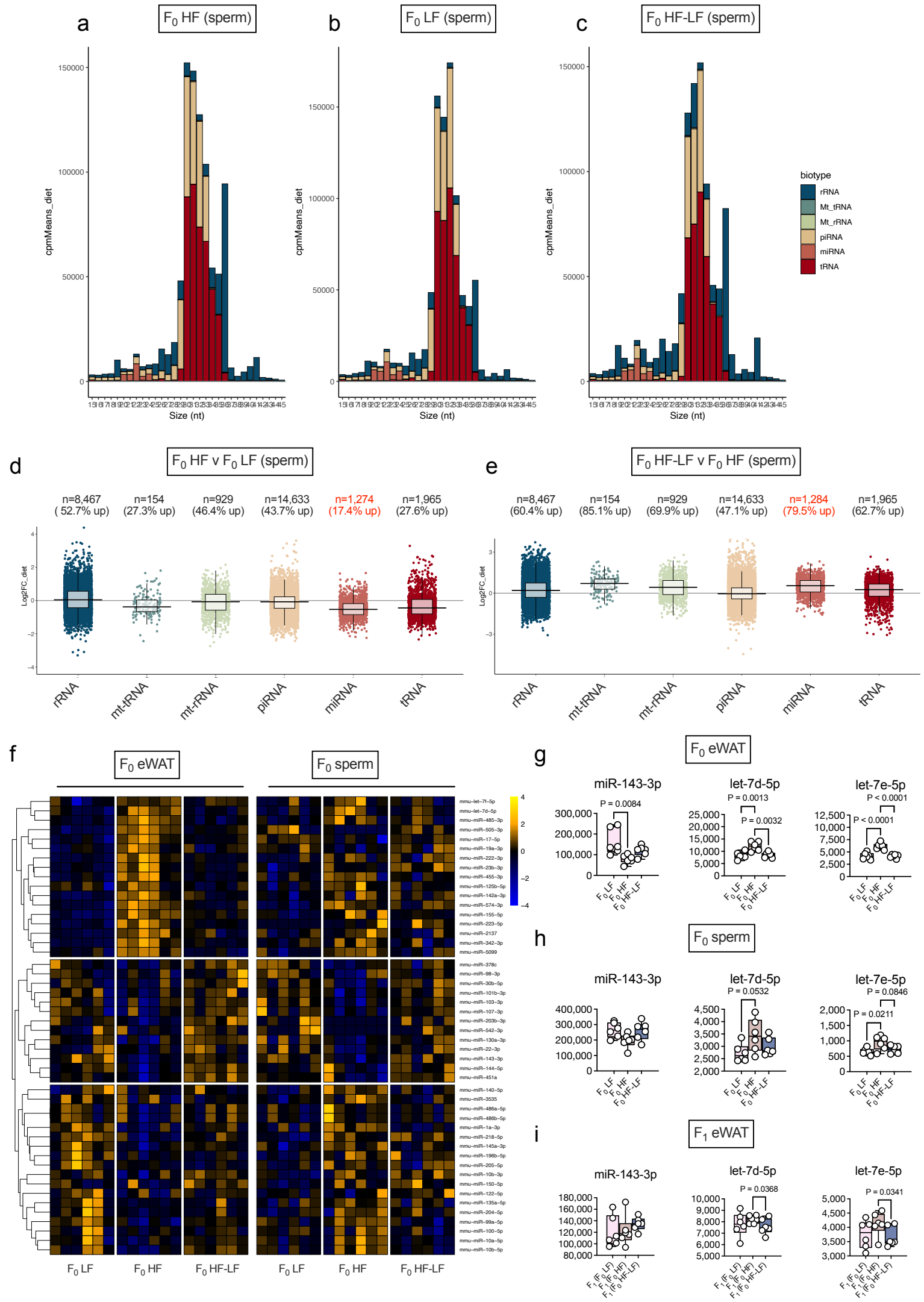

Figure 4: Zygotic delivery of *let-7d/e-5p* causes glucose intolerance in sired F_{MI} mice and impairs embryonic mitochondria.

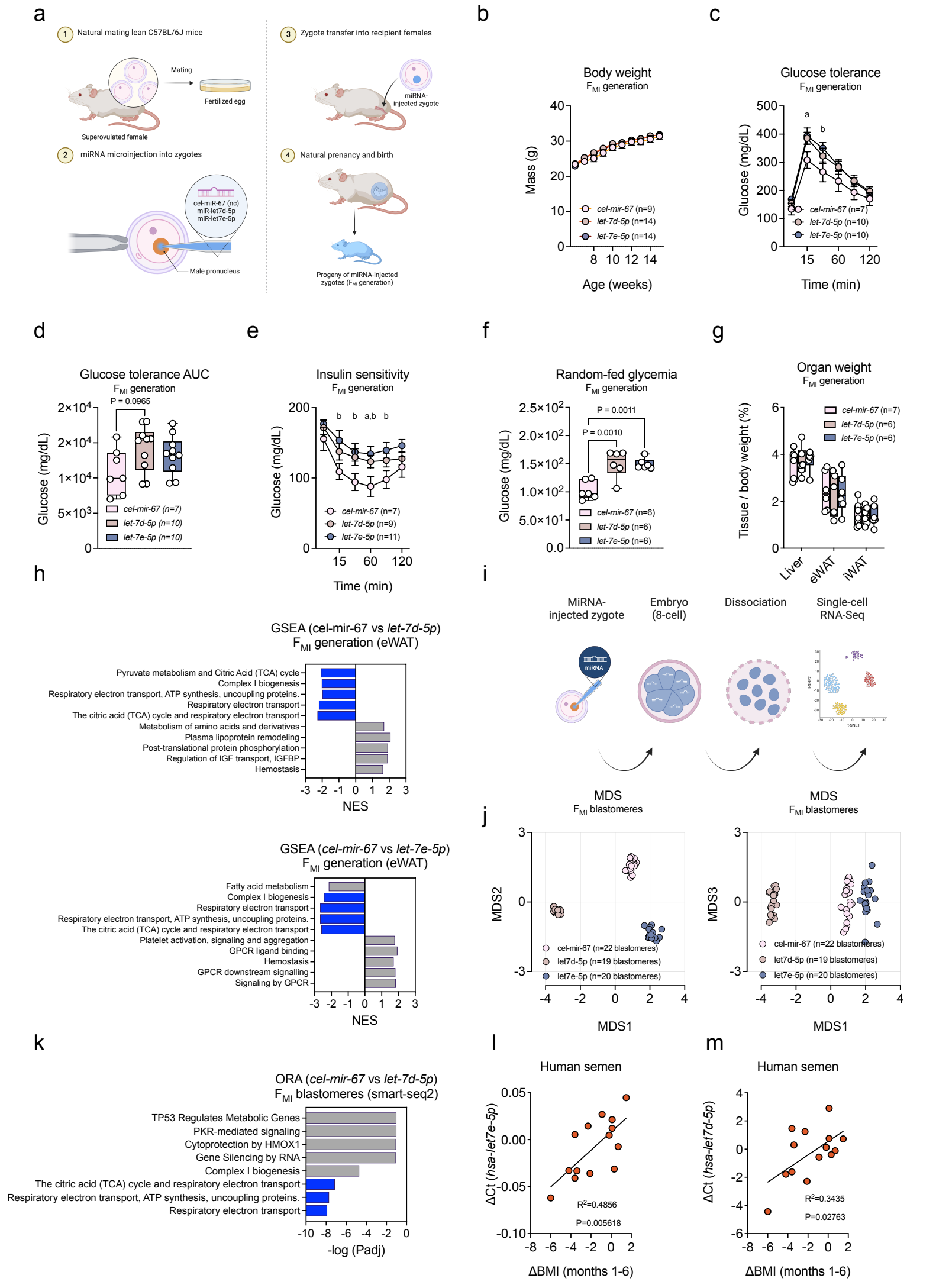

Figure 5: Adipocyte let-7 blunts mitochondrial function via a novel miR-let-7-DICER1 axis.

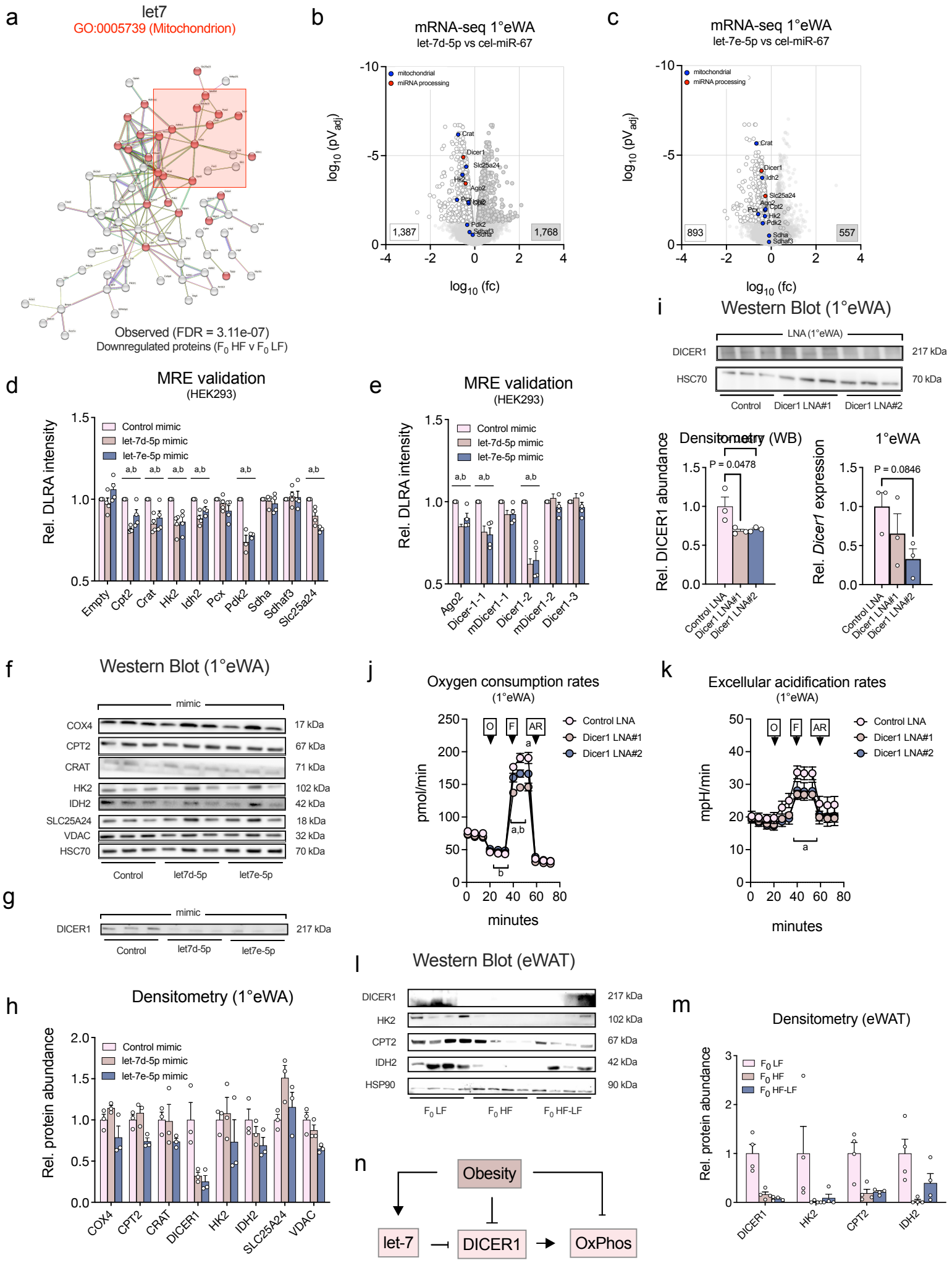

Figure S1: Paternal obesity and weight loss do not affect reproductive fitness and litter sizes

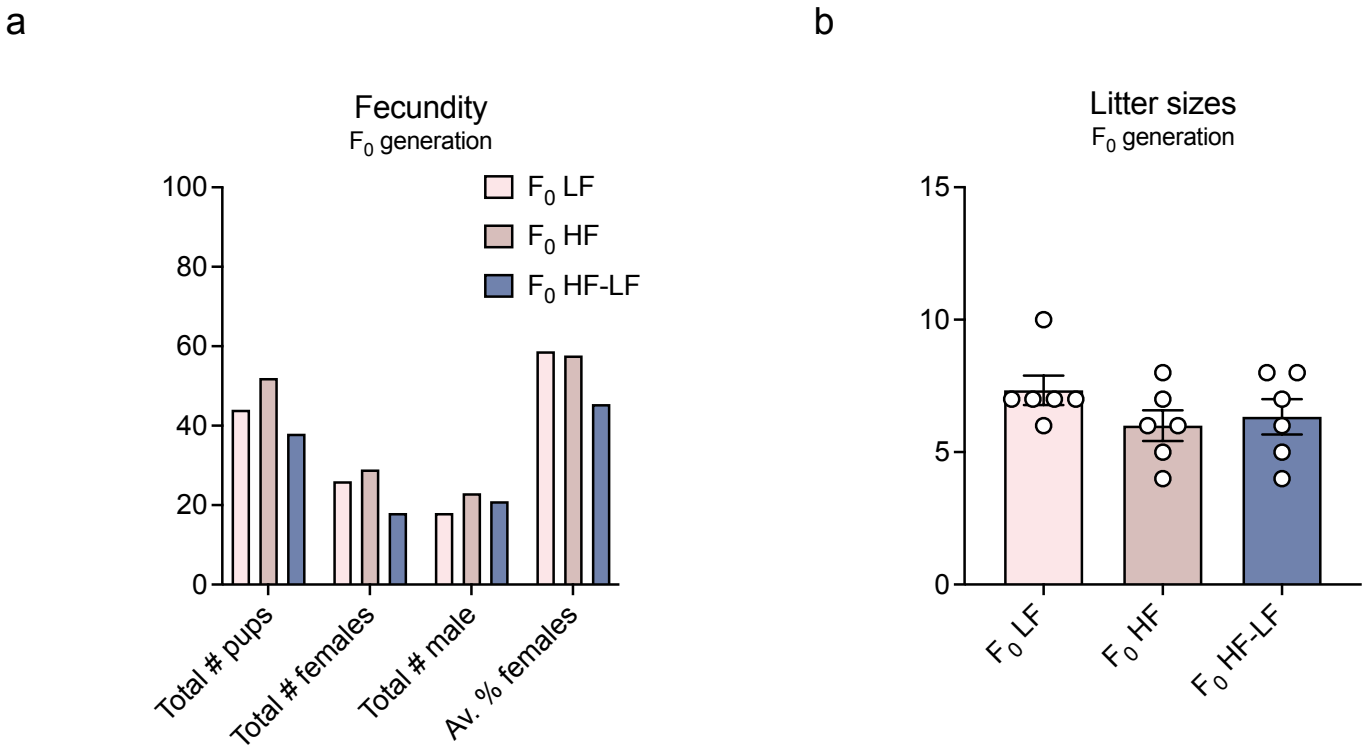

Figure S2: Paternal obesity causes heritable alterations in glucose metabolism in male but not in female mice

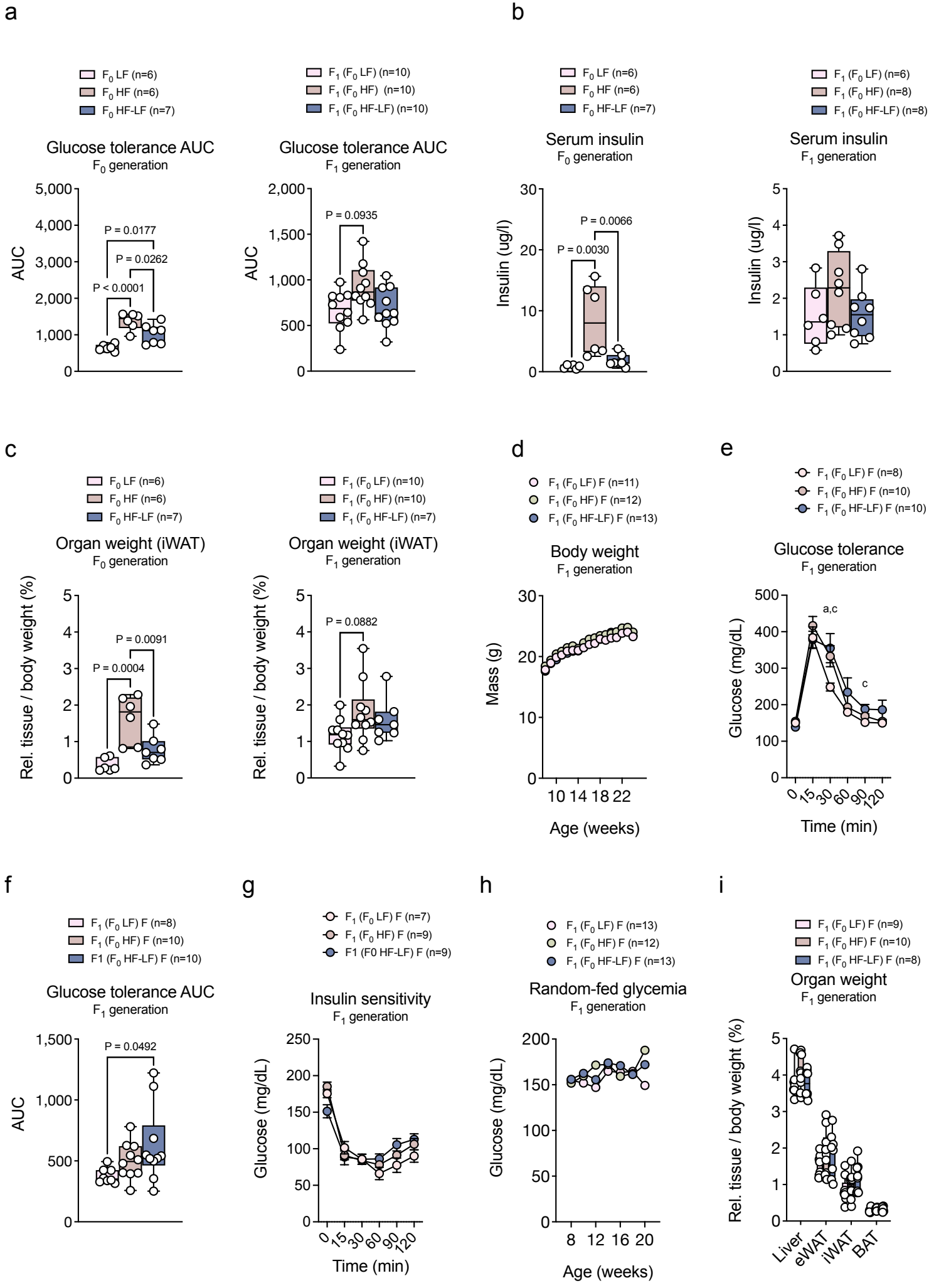

Figure S3: Effects of paternal obesity on F_0 and F_1 eWAT proteomes

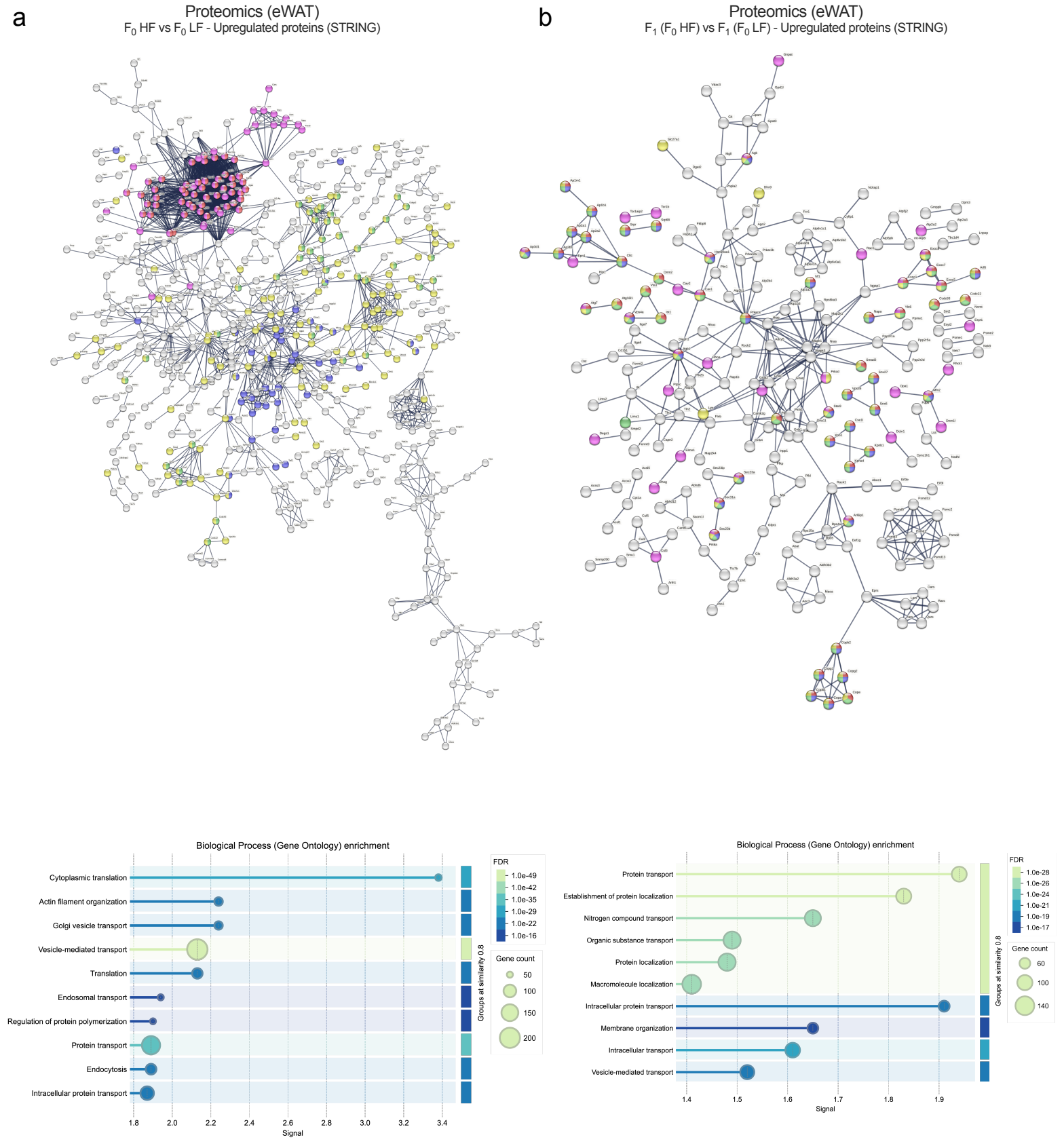

Figure S4: Paternal obesity elicits alterations in circulating mitochondria-associated metabolites and lipids

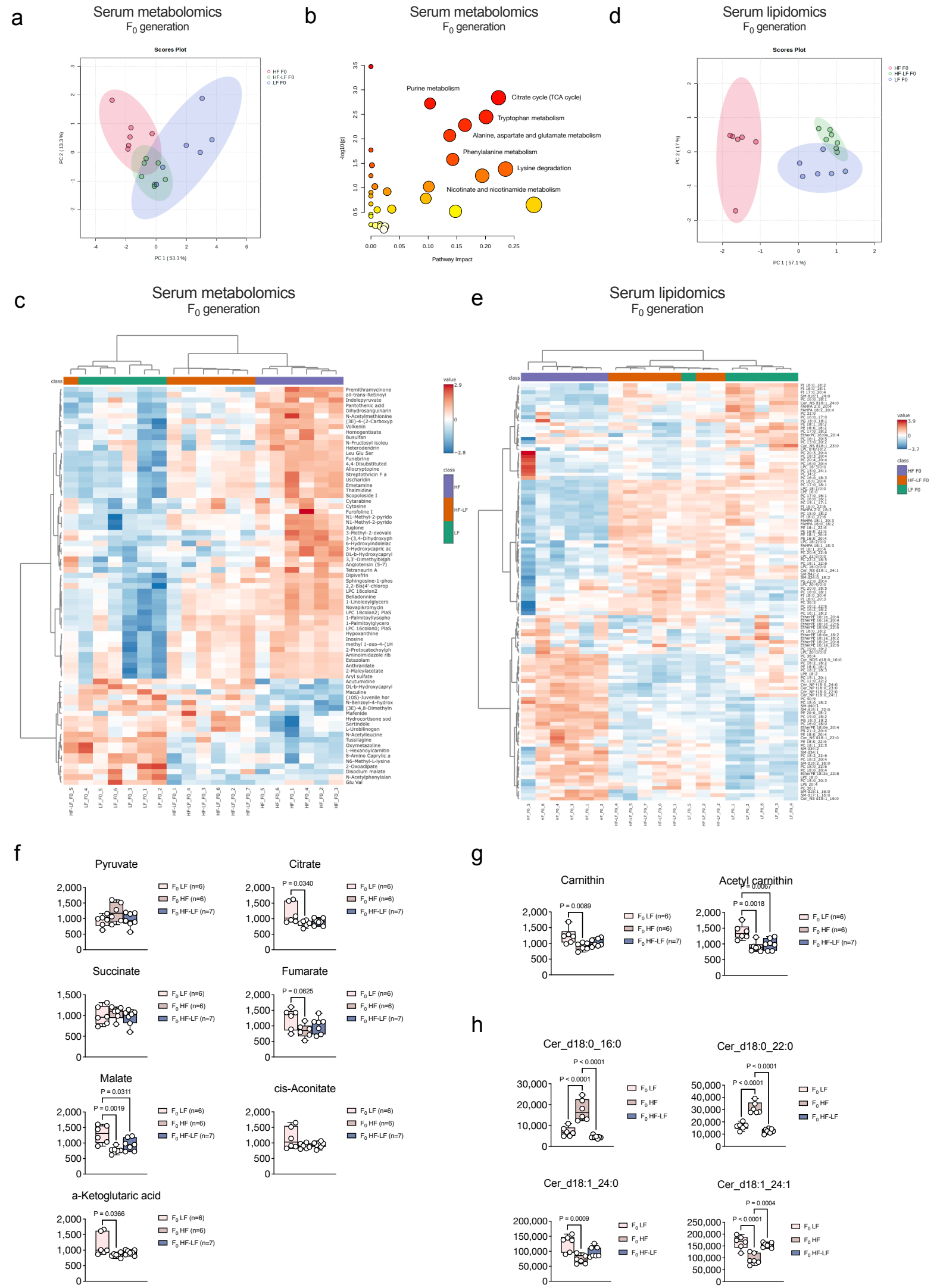

Figure S5: Paternal weight loss corrects obesity-associated mitochondrial dysfunction in eWAT.

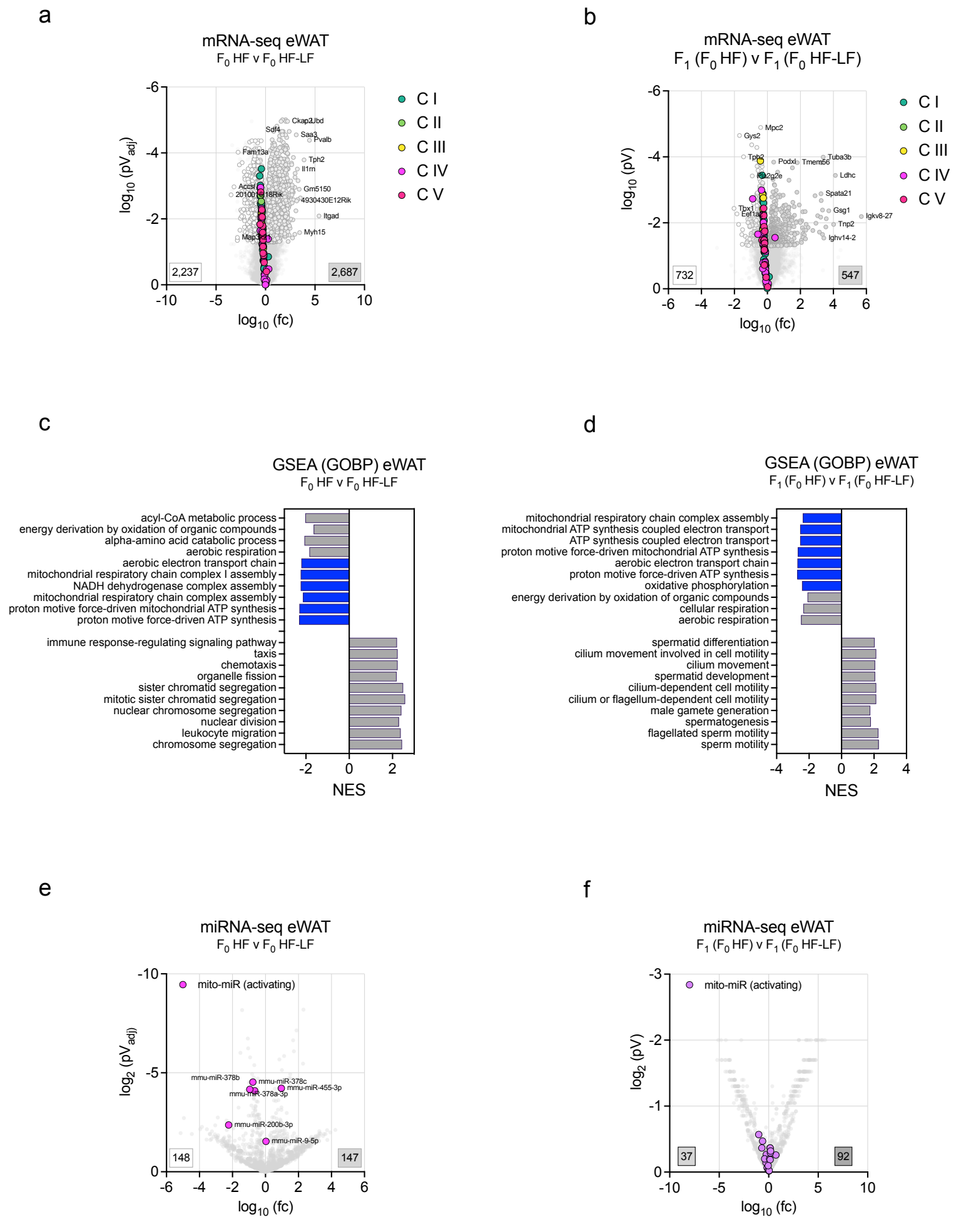

Figure S6: Paternal obesity does not affect F_1 adipose miRNA expression and meta-inflammation

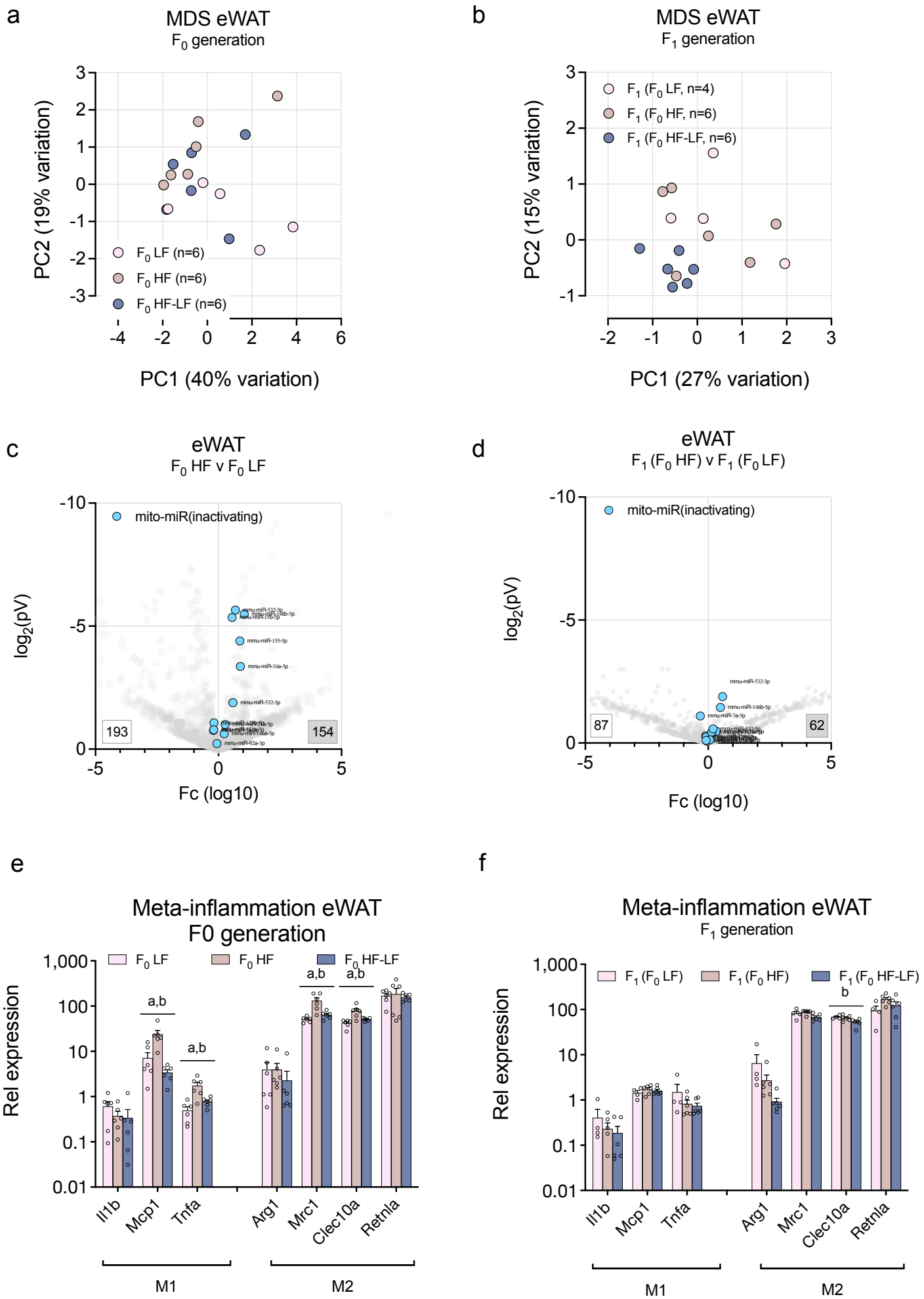

Figure S7: Paternal obesity does not affect mitochondrial gene expression in F_0 and F_1 liver

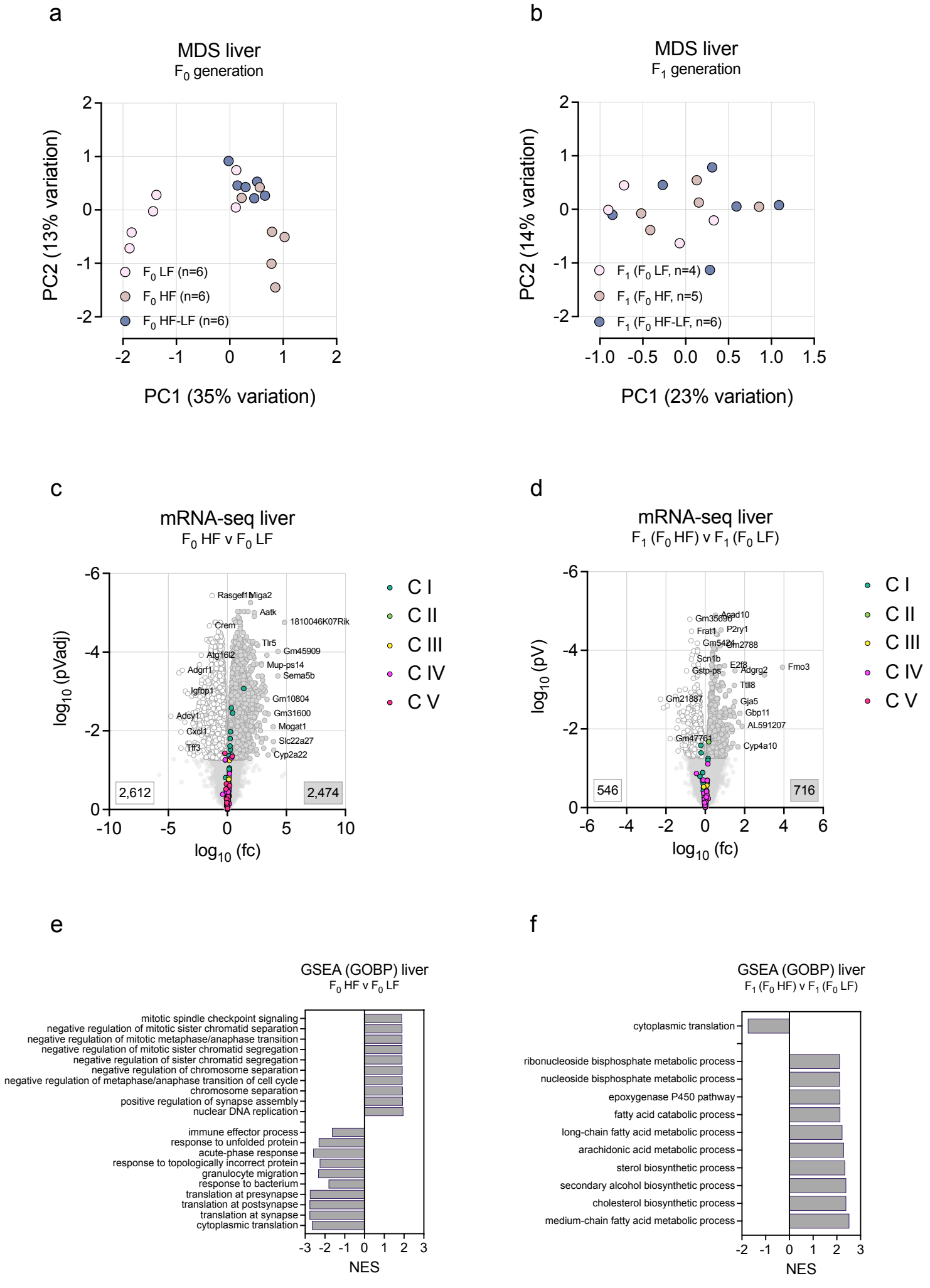

Figure S8: Paternal obesity and weight loss do not affect liver morphology and lipid metabolism in F_1 progeny

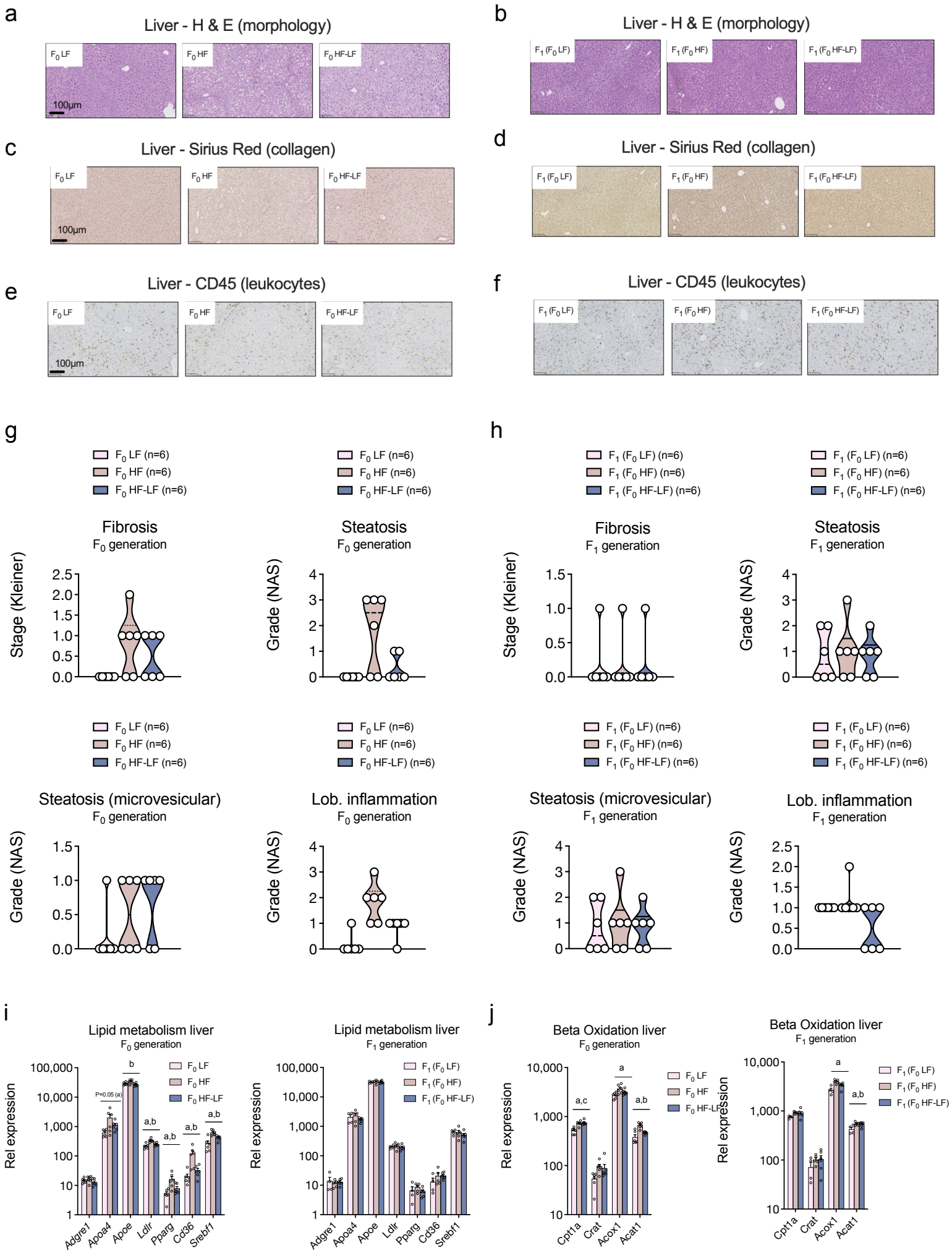

Figure S9: Paternal obesity and weight loss cause only modest changes in spermatozooa mitochondrial tRNA fragments

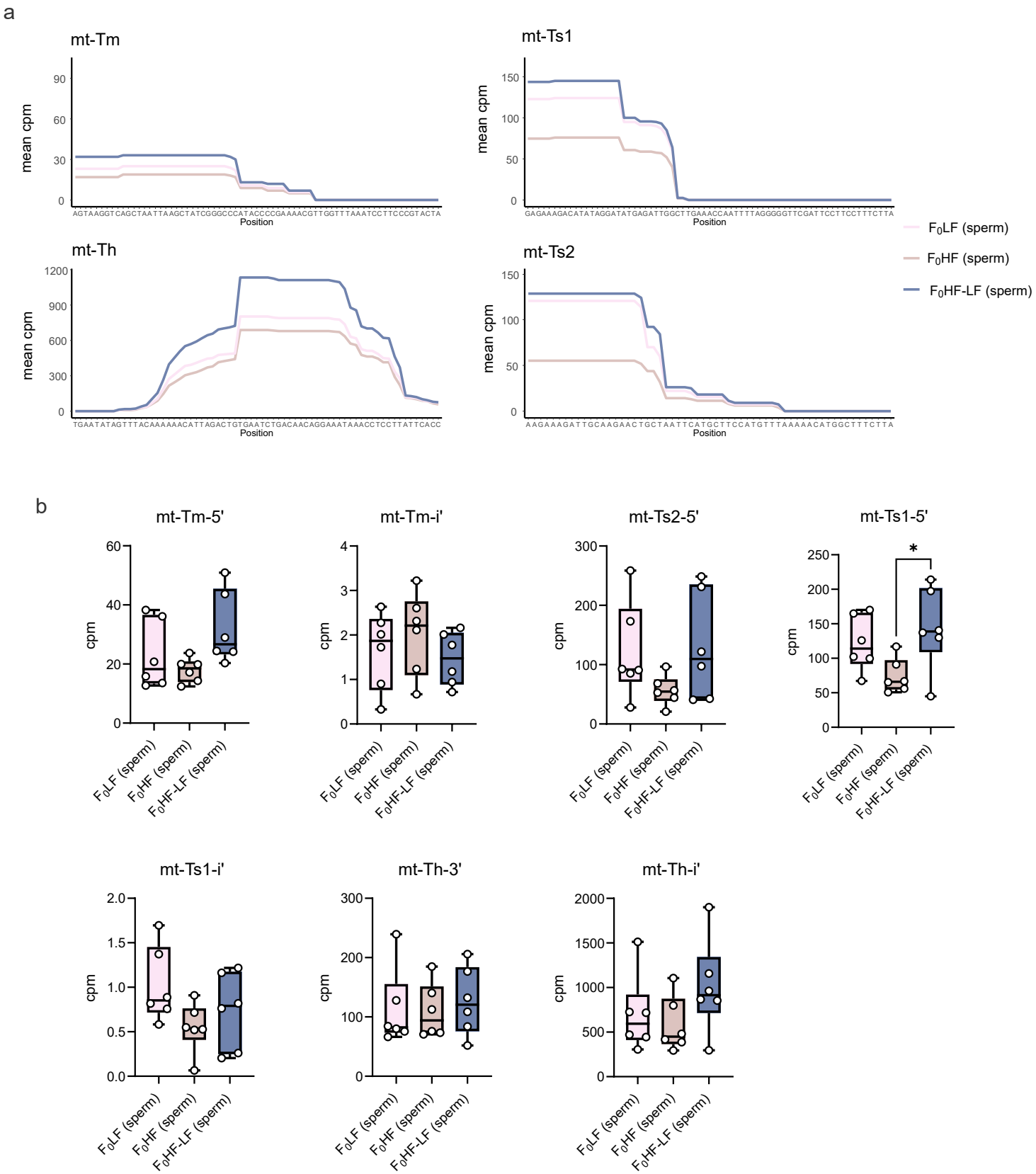
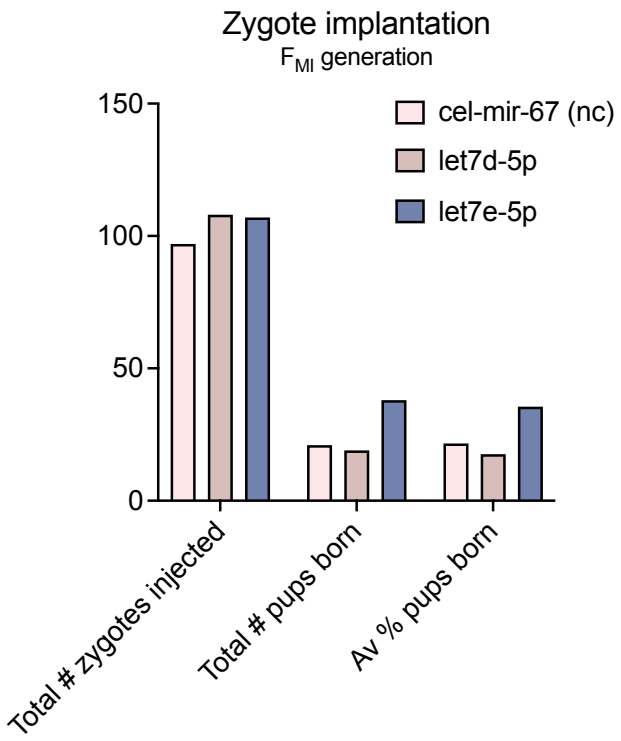
Figure S10: Zygotic microinjection of obesity associated miR-let7 does not affect embryonic viability and implantation